



**University of
Zurich**^{UZH}

Gletschertöpfe Gibel: investigation of ice-age glacial potholes

GEO 511 Master's Thesis

Author

David Wehrli
17-729-203

Supervised by

Dr. Martin Lüthi
Lukas Inderbitzin (lukas.inderbitzin@sz.ch)

Faculty representative

Prof. Dr. Andreas Vieli

30.09.2023

Department of Geography, University of Zurich

Abstract

Potholes are fluvial erosion features formed due to sediment which gets trapped in vortices and eddy currents in a water stream. This process leads to the circular shape with smooth abrasive walls potholes are known for. On a hill near the town of Schwyz called Gibel large potholes are found. However, the Gibel is a forest karst region with no permanent surface water streams. Further, the size of the potholes make formation due to rain improbable. A further mechanism which is forming potholes is subglacial water. During the last glacial maximum (LGM) glaciers reached far into the alpine foreland of Switzerland. Hence, the Gibel was covered with ice during this time. This thesis aims to get a better understanding of the formation processes of the potholes on the Gibe during the LGM. Therefore, the pothole locations were mapped. Of three well preserved potholes LiDAR scans and photogrammetric 3D-models were made. Further sediment core samples were taken. The glaciation over the Gibel was modelled, using the Instructed Glacier Model (IGM) with different fixed equilibrium line altitudes (ELA) and the climate reconstruction of the EPICA. Using the subglacial hydraulic potential subglacial water pathways were modelled. Further the strain rate is used as an indicator for glacial crevasse fields where surface water infiltrates the glacier. The results presented in this thesis indicate that the subglacial drainage system of the Muota valley discharged over the Gibel during multiple stages of the last glacial cycle. Furthermore, the pothole location on the Gibel led to a decreased sediment load in the subglacial water minimizing the material available to fill the potholes.

Contents

List of figures	3
List of Tables.....	4
1 Introduction	5
1.1 Pothole formation.....	5
1.2 Subglacial water and erosion	5
1.3 The central Swiss Alps during the ice age	6
1.4 Research question.....	6
2 Study site.....	6
2.1 Geology.....	7
3 Methods	10
3.1 Data collection (Morpho).....	10
3.2 Model work.....	11
4 Pothole Morphology	13
4.1 Results.....	13
4.1.1 Pothole 1	14
4.1.2 Pothole 2	18
4.1.3 Pothole 3	18
4.2 Discussion	19
4.2.1 Sinkhole vs Pothole.....	19
4.2.2 Pothole evolution	20
4.2.3 Sediment filling.....	20
5 Model work	21
5.1 Results.....	21
5.1.1 Ice extent and thickness	21
5.1.2 Ice surface Velocity.....	23
5.1.3 Flow direction and sediment transport	24
5.1.4 Strain rate	25
5.1.5 Hydraulic potential	26
5.1.6 EPICA Run	29
5.2 Discussion	30
5.2.1 Subglacial Waterflow	30
5.2.2 Muota valley Lake.....	30
5.2.3 Sub- and Supraglacial sediments	30
5.2.4 Comparison to Geomorphological data and other models	31
5.2.5 Model stability and accuracies	32
6 Conclusion.....	34
7 Acknowledgments.....	34
8 Bibliography	34

List of figures

Figure 1: Geological map of the Gibel (Source is the Geological atlas of swisstopo (GA25)).....	8
Figure 2: Legend to the geological map in figure 2 and figure 4	9
Figure 3: Front to back view into pothole 1	9
Figure 4: Potential potholes (marked with red circles) around pothole 1 and 3 on a hill shaded map of the Swissalti3D DEM.....	10
Figure 5: Pothole/scour form location (yellow dots), closely inspected potholes (red dots), clusters (white circles), geological faults (dark red lines), Background map is the Geological Atlas of swisstopo (GA25).....	12
Figure 6: Top (6.1) and front (6.2) view of a scour form at cluster B with visible wall collapse. The blue line indicates the top edge of the scour form. 6.3 scour form at cluster B. 6.4 over eroded scour form at cluster B.....	13
Figure 7: Solid photogrammetric model of pothole 1 with sub potholes indicated (black circles) front of the pothole to the left.....	14
Figure 8: Photogrammetric model of the back wall of pothole 1. Colour shaded (top), nonshaded (bottom). Red dashed line indicates the area of smooth fluvial erosion. Yellow line indicates a crack.....	15
Figure 9: Photogrammetric model of the left sidewall of pothole 1	16
Figure 10: Right picture: Top 80cm of bore core 1 (left), empty bore core (right). Left picture: Bore cores of bore hole 1, depth increases from right to left.....	17
Figure 11: Top view of 3D-model of pothole 2. The frontside of the pothole is to the right. The red dashed line indicates the circumference at the top of the pothole. The blue dashed line indicates the circumference at the height of the sediment filling. The blue dot is the view point of Figure 13.	18
Figure 12: Pothole 3 photogrammetric model top view. Coloured model (right), uncoloured model (left). Blue line indicates the flow direction of the water.	19
Figure 13: Backwall of pothole 2. The red and blue dashed lines indicate the top and bottom edge as in Figure 11	21
Figure 14: Thickness of the Reuss and Muota glaciers after 5000-year advance model run with a fixed ELA at a resolution of 200 m. The red circle annotates the Gibel.	22
Figure 15: Modelled surface ice velocity of the Muotathal area with different ELA heights at a resolution of 200 m.	23
Figure 16: Thickness of the Reuss and Muota glaciers after 5000-year advance model run with a fixed ELA and a resolution of 200 m. The red circle annotates the Gibel.	24
Figure 17: Modelled maximum surface strain rate in the Muotatal region with different ELA heights at a resolution of 200 m.	25
Figure 18: Subglacial water pathways (red) based on the hydraulic potential at the glacier bed calculated using the fixed ELA model runs 200 m resolution.....	26
Figure 19: Subglacial water pathways (red) based on the hydraulic potential at the glacier bed calculated using the fixed ELA model runs 100 m resolution.....	27
Figure 20: Subglacial water pathways (red lines) based on the hydraulic potential calculated using the 1460 m a.s.l. ELA 100 m resolution IGM run at two different times.	28
Figure 21: Ice thickness at different points in the study area during EPICA model runs using a current day ELA of 21.1) 3000 m a.s.l., 21.2) 3250 m a.s.l. and 21.3) 3350 m a.s.l.	29
Figure 22: Possible maximum extend of the Muotavalley lake (dark blue) during the glacier retreat after the LGM. The subglacial water pathways (red) and the glacial thickness are shown (ELA 1800).	31
Figure 23: Comparison between model runs at a resolution of 100m (top) and 200m (bottom).	33

List of Tables

Table 1: Most important variables used for the model runs 12
Table 2: Soil profile form bore core 1 16
Table 3: Pothole measurements 19

1 Introduction

Potholes are erosion features known for their circular form and smooth abrasive walls. As a fluvial erosion form potholes are most often found in rivers flowing over bedrock. However, that are not the only places where potholes can be located. They are also occurring at coasts and on hillslopes (Ji, Li and Zeng, 2018). In rivers they can be a main driver for rock incisions, creating deep, tight gorges (Hancock, Anderson and Whipple, 1998; Das, 2022). Besides being an indicator for active erosion in for example rivers, potholes are also witness of past fluvial erosion as seen for example in glacial potholes (Keller, 2021).

In Switzerland glacial potholes are found in multiple locations for example on the Maloja pass or near the Gorner glacier in Zermatt (Maisch, 2009). One of the best known and best studied places with glacial potholes is the “Gletschergarten” in Luzern. There potholes were discovered in sandstone beneath sediment and humus while building a wine cellar. The formation of the potholes in Luzern can be traced back to the last glacial period (Keller, 2021). However, most of the pothole sites in Switzerland are less to not mentioned in the scientific discourse, as are the potholes on the Gibel. The potholes found on the Gibel likely also formed during the last glacial period, when the Reuss and Muota glacier reached far into the lake basin of the Vierwaldstättersee and Zugersee and beyond (e.g. Bini *et al.*, 2009; Reber *et al.*, 2014; Seguinot *et al.*, 2018).

1.1 Pothole formation

The formation of glacial potholes was long believed to be the result of water plunging down through moulins and glacier crevasses directly down to the bedrock beneath the glacier where it would erode the rock like a waterfall. However, as Alexander (1932) states in his paper this seems not feasible due to the necessity of a stationary glacier. Current knowledge states that subglacial potholes form in subglacial channels similar to potholes in caves and in rivers, where eddy currents and the vortexes trap sediments, pebbles and cobbles to grind out the potholes (e.g. Alexander, 1932; Lorenc, Barco and Saavedra, 1994; Hancock, Anderson and Whipple, 1998; Das, 2022). These eddies occur due to impurities in the bedrock in form of cracks, folds and joints (Das, 2022) or at knickpoint where flow separation occurs (Hancock, Anderson and Whipple, 1998). The study of river pothole sites, with still active erosion, can give an insight into the processes which lead to the formation of glacial potholes (Higgins, 1957). Ji, Li and Zeng (2018) found that the ratio between pothole diameter and pothole depth is an indicator for the type of grinder used to carve out the pothole. The size of potholes can further be an indication of the water flow depth and hydraulic potential gradient on the site during formation. Deeper flow depths or steeper gradients lead to the formation of bigger potholes (Pelletier *et al.*, 2015). The time it takes to form a pothole varies due to factors such as flow rate, grinder abundance and bedrock hardness. While in Sandstone potholes of 6m diameter and 5m depth can form over the span of 85 years, it is assumed that in hard rock the formation of potholes takes hundreds to thousands of years (Wohl, 1998). However in a more recent study Kale and Joshi (2004) found that in granitic rock potholes can also form within a human lifespan. Further, Gilbert (2022) suggests in his study that glacial potholes with a diameter up to two meters can be carved out in the time span of a single large outburst flood event.

1.2 Subglacial water and erosion

Glacial potholes are formed due to subglacial water flows. Therefore, the understanding of subglacial water movement is important to get a better understanding of the formation of glacial potholes. Subglacial water systems can be divided into an efficient, channelised system and an inefficient, distributed system (Werder *et al.*, 2013). The channelized system can be divided further into R-

channels which are growing into the glacier and N-channels which are ground into the glacier bed (Fagherazzi *et al.*, 2021). N-channels form when the erosion rate of subglacial water flow is higher than the erosion by ice creep. These subglacial channels play an important role in pothole formation (Fagherazzi *et al.*, 2021; Gilbert, 2022). The pathway and catchment area of subglacial channel system before the potholes give an insight about the conditions leading to the formation of the potholes. To get an idea about the form of a subglacial water system modelling is often used. These models range from relatively simple calculations of the hydraulic potential (Shreve, 1972) to models dividing the subglacial environment into a channelized and distributed system and taking into account water inputs and englacial storages among other variables (Werder *et al.*, 2013).

1.3 The central Swiss Alps during the ice age

During the last glacial maximum (LGM) the Alpine glaciers reached out far into the forelands (Bini *et al.*, 2009). Witnesses of this glaciation concerning the Reuss glacier are moraines found as far from the alps as Birr (Kt. Aargau), approximately 45 km away from the Alps (Kamleitner *et al.*, 2023). Reber *et al.* (2014) used erratic boulders found on the Rigi north slope and near Lenzburg to reconstruct the retreat of the Reuss glacier after the LGM. The start of the retreat was dated to 22.2 ± 1.0 ka BP (Reber *et al.*, 2014) with the latest bigger readvance 20.8 ± 1.3 ka BP up to Bremgarten (Kt. Aargau) (Kamleitner *et al.*, 2023). Hantke, Pfiffner and Gouffon (2013) concluded that the lower Muota valley had a maximum ice height of 760 m a.s.l. $19\,185 \pm 245$ years BP, due to the finding of a bear teeth in the Lauiloch (CRS: LV95: 2697.0/1205.3) which was dated to this time.

Seguinot *et al.* (2018) used the Parallel Ice Sheet Model (PSIM) in combination with the climate inferred from the European Project for Ice Coring in Antarctica (EPICA) to model the last 120 ka of glaciation in the European alps at a resolution of 1 km and 2 km. According to the model the maximum extent of the Reuss glacier occurred approximately 24 ka BP. A second readvance into the Alpine foreland is modelled approximately 19 ka BP.

1.4 Research question

The goal of this thesis is to get a better understanding of the condition leading to the pothole formation on the Gibel. This is accomplished by trying to answer these three questions:

- What were the glacial conditions over the Gibel during the last glaciation?
- Where did subglacial water flow through in the Muota valley region during the last glaciation?
- How do the potholes on the Gibel compare to other potholes found in the world?

These questions are answered in two steps. First, the location of the potholes was mapped, and 3 Potholes were examined in more detail. Then the waterflow during the glaciation of the Gibel was modelled using the Instructed Glacial Model (IGM) and the hydraulic potential.

2 Study site

The study area is located on a hill named Gibel in the northern Alps of Switzerland. The Gibel forms a barrier to the entrance of the Muota valley as the orographic right flank of the Muota-Schlucht. This is a narrow gorge, deeply incised into the bedrock. To the north and west of the Gibel the wide valley of the town of Schwyz and Brunnen opens up. To its northeast and east the Rotenflue (1571 m a.s.l.) and Vorderer Oberberg (1207 m a.s.l.) rise. In the southeast the Muotatal widens upstream.

The previously mentioned Muota-Schlucht south of the Gibel is further confined by the Stoos (1272 m a.s.l.) on its orographic left side. The Gibel is a typical forest karst region. There are no permanent

surface streams found on the hill and discharge is assumed to happen through sub surface flow. Lying in the northern Alps the climate over the Gibel is temperate and has 4 noticeable seasons. There is on average between 1300 mm and 1500 mm precipitation per year with a slightly higher amount of precipitation during the summer months (Meteo Schweiz, no date).

The pothole area is approximately 300m above the valley floor (roughly 750 m a.s.l.) on the north to northeast side of the Gibel. The potholes are all linked to faults in the bedrock. The more closely inspected potholes are found in a “valley” which divides the Gibel into an east part and a west part. They are all found on the eastern part or in the “valley”.

2.1 Geology

The Gibel is part of the “Drusberg-Decke” a sub slab of the upper Helvetic slab (Faber *et al.*, 2003; Hantke, 2022). In the following it will be described where the slabs composing the “Drusberg-Decke” are found on the Gibel. On the north and west side of the Gibel, Schrätenkalk (biomicritic limestone) is the upper most rock layer. As a limestone formation it is prone to karst formation. At the upper south facing slope of the Gibel the Garschella-Formation is the uppermost rock layer. It consists out of the Brisi-Member which is a glauconitic clayey sandstone and biotrital limestone layer visible on the upper part of the slope and an the overlaying Selun-Member which consists out of glauconitic sandstone, limestone banks and phosphorite layers. On the lower eastern part, the Seewen- and Amden-Formation are overlaying the Garschella-Formation. The Seewen-Formation consists out of limestone and marl which are also prone to karst formation. The Amden-Formation out of calcareous marl and sandstone. All sedimentary rocks were deposited during the Cretaceous period (Hantke, 2022). At the foot of the Gibel the Rock is mostly overlayed by a sedimentary layer deposited during the Quaternary period. Further, quaternary ice-age moraines cover mostly the northeastern part of of the Schrätenkalk formation. Further moraine deposits are found at the southern entrance to the “valley” which divides the Gibel into a western and an eastern part, and around the village Ufiberg (see Fig. 1).

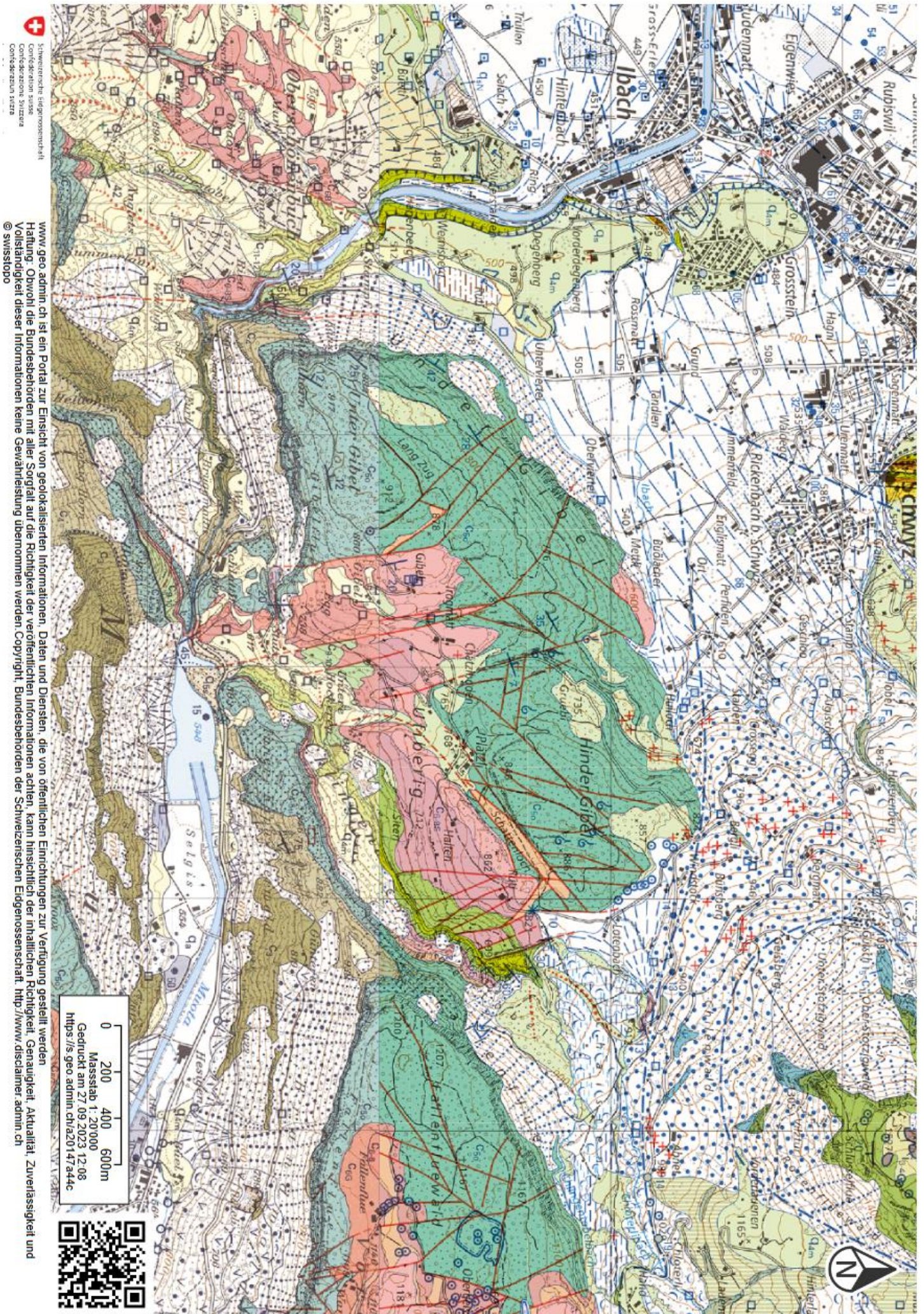


Figure 1: Geological map of the Gibel (Source is the Geological atlas of swisstopo (GA25))

www.geo.admin.ch ist ein Portal zur Einsicht von geokalibrierten Informationen. Daten und Diensten, die von öffentlichen Einrichtungen zur Verfügung gestellt werden.
 Haftung: Obwohl die Bundesbehörden mit aller Sorgfalt auf die Richtigkeit der veröffentlichten Informationen achten, kann hinsichtlich der inhaltlichen Richtigkeit, Genauigkeit, Aktualität, Zuverlässigkeit und Vollständigkeit dieser Informationen keine Gewährleistung übernommen werden. Copyright, Bundesbehörden der Schweizerischen Eidgenossenschaft. <http://www.swisstopo.ch>

Schweizerische Eidgenossenschaft
 Confédération suisse
 Confederazione Svizzera
 Confederaziun Svizra

Quartär

	Künstliche Aufschüttung, Auffüllung
	Künstlich verändertes Gelände
q _a	Rezente Alluvion
	Sumpf, Ried / idem, drainiert
	Torfmoor / idem, drainiert
q _L	Hanglehm
q _b	Bachschutt
	Bachschuttkegel
	Gemischter Schuttkegel: Bach-, Murgang- und Hangschutt
	Hangschuttkegel / Hangschuttschleier / Hangschutt (mit Blockschutt)
	Fels- bzw. Bergsturزابlagerung, Blockschutt, z.T. mit Hangschutt
	Ophiolithschutt (südwestlich der Mördergrube)
	Rutschmasse / idem, mit Darstellung der betroffenen Formation
	Sackungsmasse (mit Darstellung der betroffenen Formation)
	Zerrüttete Sackungsmasse
q _{SL}	Seebodensedimente (nur in Bohrungen aufgeschlossen)
q _{ST}	Trachslau-Schotter: grauer Schotter, meist von geringmächtigen Seeboden- und Verlandungssedimenten bedeckt
	Spätglazialer Bachschuttkegel
q _s	Letzteiszeitlicher Schotter, undifferenziert
q _{sN}	Niderstalden-Schotter
q _{lm}	Lokalmoräne (Till)
	Moränenwall
q _{4m}	Letzteiszeitliche Moräne (Till)
	Moränenwall
q _m	Moräne (Till) älterer Eiszeiten

Drusberg-Decke

P a l ä o g e n	P r i a b o n i e n	e ₃	Stad-Formation: hellgrauer bis gelblichgrün anwitternder glimmerreicher Tonstein	} Spirstock-Member	
		e _{60a}	Plattiger quarzreicher, mittel- bis grobkörniger Sandstein, an der Basis brekziös («Obere Sandsteine»)		
		e _{60b}	Dunkelgrauer, teils grünlich-gelblich anwitternder siltiger Mergel mit Blöcken und Geröllen («Blockmergel»)		
		e _{60c}	Plattiger Quarzsandstein, grobkörniger kalkiger Sandstein, Feinbrekzie und sandig-siltiger Mergel; mit Blöcken aus Euthal-Formation («Untere Sandsteine»)		
	K r e i d e	Y p r e s e n	e ₃	Euthal-Formation: grauer, Nummuliten führender Kalk, glaukonitisch-phosphoritischer spätiger Kalk	
			C ₁₂₋₁₃	Wang-Formation: dunkelgrauer bis schwarzer, meist kieselig, teils glaukonitischer Kalk und Kalkmergel, z.T. schiefrig	
		C é n o m a n - M e s s i n g	C ₁₁₋₁₂	Amden-Formation: dunkel- bis rauchgrauer, teils siltig-sandiger kalkreicher Mergel, Glaukonit führende Sandkalkbänke	
			C ₉₋₁₀	Seewen-Formation: hellgrauer, weiss anwitternder dünnbankiger, teils knollig-faseriger mikritischer Kalk mit schwärzlichen Mergelzwischenlagen	
			C _{8-8S}	Selun-Member: glaukonitischer Sandstein, Kalkbänke und -knollen, Phosphoritlagen	} Garschella-Formation
		C _{8B}	Brisi-Member: glaukonitischer toniger Sandstein, biodetritischer Kalk		
C _{8L}		Gams-Schichten: feinkörniger bioturbierter Sandstein			
A p t i e n - A l b i e n		C _{6G}	Luitere-Bank: Sandstein mit Phosphoritknollen	} Schratenkalk-Formation	
		C _{6G}	Grünten-Member («Obere Orbitolinenschichten»): grünsandiger Mergel bis sandiger Kalk; zuoberst Glaukonit führender spätiger Kalk		
		C ₅₀	«Oberer Schratenkalk»: hellgrau anwitternder massiger biomikritischer Kalk		
B e r r i e n	C ₅₀	Rawil-Member («Untere Orbitolinenschichten»): Wechsel-lagerung von rötlich braun anwitterndem, z.T. sandigem Kalk und bräunlichem fossilreichem Mergelkalk	} Schratenkalk-Formation		
	C ₄₉	«Unterer Schratenkalk»: hellgrau anwitternder massiger biomikritischer Kalk			
	C ₄	Drusberg-Member: Wechsel-lagerung von dunklem kalkigem Mergel und dunkelgrauem mergeligem, teils knolligem Kalk	} Tierwis-Formation		
	C ₃	Altmann-Member: glaukonitischer, rostig anwitternder Kalk mit Phosphoritknollen			
	H a u t	C ₃	Helvetischer Kieselkalk: dunkelbraun anwitternder gebankter, kieselig spätiger Kalk mit vereinzelten schiefrigen Mergellagen		
	V a l a n g i n i e n	C _{2D}	Diphyoides-Kalk: blass gelbgrau anwitternder plattiger biomikritischer Kalk und grauer schiefriger Mergel		
		C _{2V}	Vitznau-Mergel: Kalk-Mergel-Wechsel-lagerung (durch quartäre Ablagerungen verdeckt)		
B e r r i e n	C _{1P}	Palfris-Formation: dunkelgrauer siltig-sandiger bis toniger Mergel			

Figure 2: Legend to the geological map in figure 2 and figure 4



Figure 3: Front to back view into pothole 1

3 Methods

To get a better understanding of the potholes on the Gibel, the thesis was divided into two parts. In a first step a geomorphological and descriptive survey of the potholes was conducted focusing on three well preserved potholes. In a second step the Muota and Reuss glacier were modelled reaching over the Gibel to get an understanding of the conditions during the last ice age.

3.1 Data collection (Morpho)

For the geological survey data was collected during multiple field days in the autumn (Oct.- Nov. 2022). In preparation the Swissalti3D DEM (digital elevation model of Swisstopo) was inspected, and potential potholes were marked (Fig. 4). These locations were afterwards confirmed in the field with the help of a GPS. The diameter of each pothole was measured using a Laser distance meter approximately at the largest and the smallest diameters, where possible. Then, 3 easily accessible potholes were selected for further investigation. The following methods were used to get a better insight into the geomorphology of these 3 potholes.

Multiple LiDAR scans were made of each of the 3 potholes. To cover as much surface of the pothole walls as possible 4 scans in the large pothole respectively 3 scans in the 2 smaller potholes were captured. The sensor location differed for every laser scan. The scans were made using a LEICA BLK360. The resulting point clouds were cleaned up manually by removing all points representing vegetation above the pothole. Furthermore, points representing vegetation within the pothole were also removed where possible. The scans were then overlaid to get 1 point cloud for each pot. Those point clouds were then used to measure the width and wall height above the sediment filling of the potholes. The diameter and the overall pothole depth were then subsequently used to compare the potholes to pothole types found by Ji, Li and Zeng (2018).

Using photogrammetry an additional coloured 3D Model was created for each pothole using Agisoft Metashap. Depending on the pothole size photos were taken from 2-4 locations within the potholes in a circular fashion. The photos were taken using a Canon ESO 600D with a Canon ESF 18-55mm objective. The data collection was on a cloudy day for better modelling results. Furthermore, the pictures had an overlap between 60%-80%. The distance between distinct features in the potholes were measured for triangulation purposes. The coloured 3D Model were used to get a better overview of features in the potholes.

The potholes are filled with sediments. A sample drill was used to drill through the soil to the pothole floor. The drill produced soil samples of approximately 20 cm depth hence the drilling took place in 20 cm increments. In pothole 1 this was not possible since the drill was too short (ca 1.2 m). In the potholes 1 and 2 multiple drillings took place while in pothole 3 only one drilling in the middle took place. In pothole 1 additionally percussion probing was used to get the depth of the sediment. The probing location were chosen at random with a minimum distance to the wall of 1.5m.

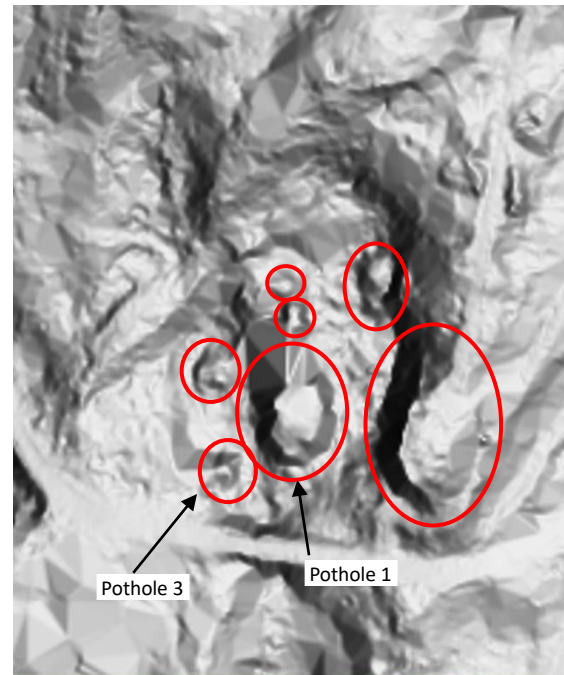


Figure 4: Potential potholes (marked with red circles) around pothole 1 and 3 on a hill shaded map of the Swissalti3D DEM.

3.2 Model work

To get a better understanding of the glaciation of the Gibel during the last Ice-Age the Reuss and the Muota glacier were modelled. For this purpose, the Instructed Glacial Model (IGM) created by Jouvét *et al.* (2021) was used. The IGM was chosen due to its capability to model large area in high resolution within a short time without needing large infrastructure. The IGM is a numerical glacial model using Convolutional Neural Network to emulate and therefore speed up the calculation of the Navier Stokes ice flow model or SIA+SSA (Jouvét *et al.*, 2021). Multiple runs were conducted using a resolution of 100 m and 200 m. Each IGM run was conducted using a fixed equilibrium line altitude (ELA). The ELA's used ranged from 1300 m to 1800 m a.s.l in 100 m steps plus runs at an ELA of 1460 and 1480 m a.s.l. The fixed ELA model runs were conducted for at least 5000 years after that the modelled glaciers were assumed to be in equilibrium. Additionally, with a 200 m resolution the model was run using the European Project for Ice Coring in Antarctica (EPICA) climate scenario between 35000 to 10000 years BP. Hereby, a current day ELA had to be given as a starting point. Start ELA's used for the EPICA runs were 3000 m, 3500 m and 3350 m a.s.l. Using the current day ELA and the EPICA climate the ELA height during the last ice age is calculated.

As input for the topography the DEM25 of Swisstopo was used and recalculated into the UTM32 coordinate system. The flow speed of the ice is controlled by a single variable which comprises the sliding coefficient c and the rate factor A in Glens flow law (Jouvét *et al.*, 2021). The model stability can be increased with the CFL-number (Courant-Friedrichs-Lewy-Number). The CFL-number is calculated using the timesteps and the resolution of the model. Since the resolution is fixed and a CFL-number is defined by the user the timestep length is automatically calculated by the IGM. For a reasonable model run time and stability a CFL-number of 0.05 was chosen. Model runs with smaller CFL-numbers needed significantly more time to run for a minimal increase in model accuracy (stability). The IGM outputs which were used for further calculations are ice thickness (thk), flow velocities ($velsurf_mag$: overall flow velocity, $uvelsurf$: x direction flow velocity, $vvelsurf$: y direction flow velocity) and glacier surface topography ($usurf$). In an effort to get closer to a realistic glacier surface the glacier thickness was smoothed using a moving average filter. A filter window of 3 was chosen so larger topographic features would not be smoothed. All input parameters used to model the glaciers are found in table X.

The formation of glacial potholes is directly linked to glacial water flow and especially to subglacial water flow. To get an understanding of the waterflow paths below the glacier the subglacial hydraulic potential:

$$\phi = \rho_i * g * (z_s - z_b) + \rho_w * g * z_b$$

was calculated. Where ρ_i is the average density of glacier ice, ρ_w is the density of water, z_s is the surface height of the glacier and z_b is the height of the underlying terrain. These calculations were made over the whole model area. The hydraulic potential maps were then used the same way as DEM's to delineate the watersheds below the glacier using the python library "pysheds" (Bartos *et al.*, 2022). This resulted in maps of subglacial flow paths.

Crevasses and moulins are an important water source to the subglacial water system especially in times when glaciers are melting (Shreve, 1972). To get an indication where crevasses have formed the strain rate can be used (Nye, 1959). The maximum extensive strain of the ice was calculated using the surface flow velocities in x and y direction by the IGM.

Also surface ice flow paths were calculated to get a better understanding of the region where the ice flowing over the Gibel originated. Therefore, multiple points on the Gibel were chosen. The ice flow was then calculated backward using the flow direction of the ice on the current time step.

The different fixed ELA model runs were then compared with each other and within different timesteps of themselves to get an understanding of the stability of the model results. Furthermore, they were compared to other model runs and geomorphological findings out of the region.

Table 1: Most important variables used for the model runs

Variable name in the model	Value	Function
cfl	0.05	
strflowctrl	100	
ela (ela0 for EPICA runs)	1300-1800 (3000-3350) m a.s.l.	
gradabl	0.0067	Sets the change in massbalance per meter height in the ablation zone
gradacc	0.005	Sets the change in massbalance per meter height in the accumulation zone
maxacc	1.0	Defines the maximum accumulation

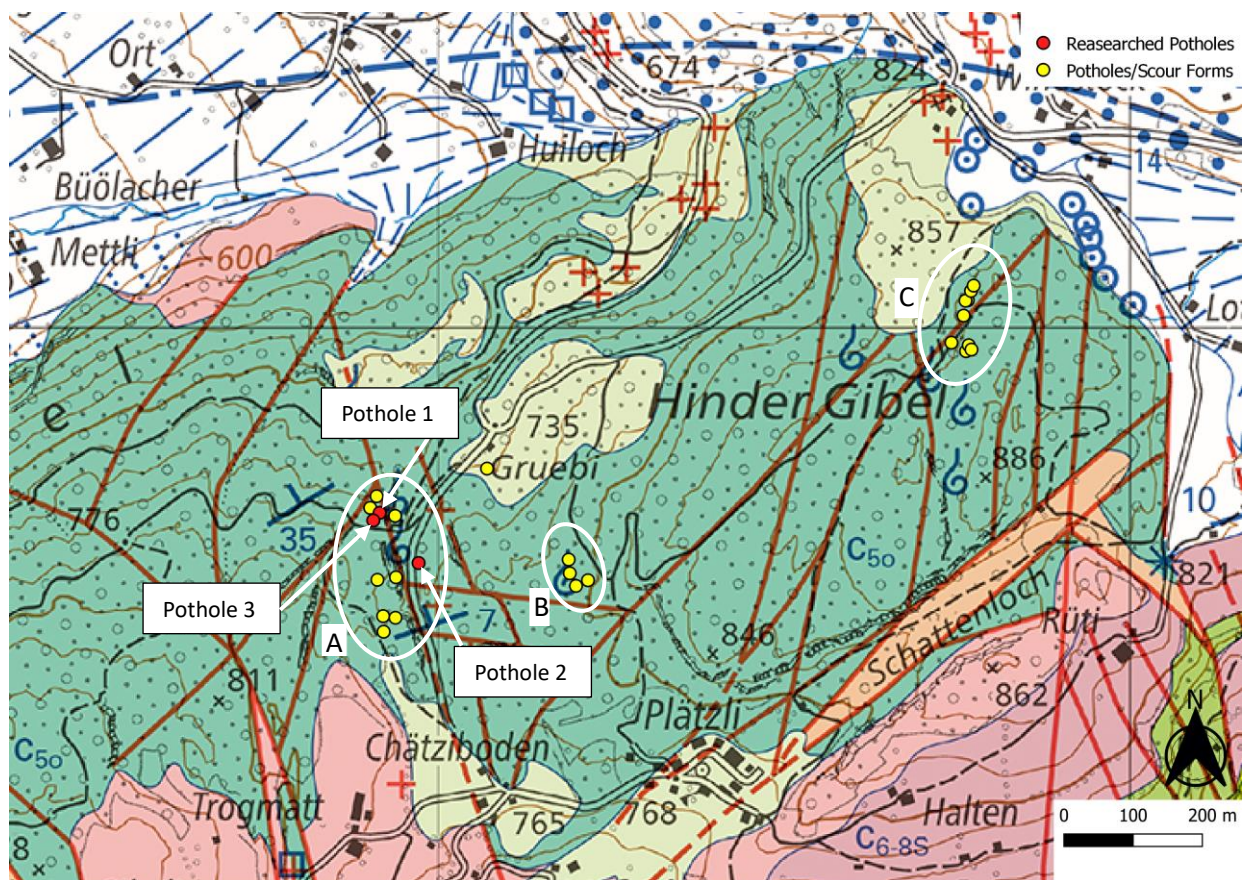


Figure 5: Pothole/scour form location (yellow dots), closely inspected potholes (red dots), clusters (white circles), geological faults (dark red lines), Background map is the Geological Atlas of swisstopo (GA25)

4 Pothole Morphology

In this section an overview of the found potholes is given, followed by a closer qualitative look at the morphology of three well preserved potholes. In a second part the found results will be discussed.

4.1 Results

On the eastern part of Gibel 23 potholes and large scour forms were found (Fig. 5). The potholes are on the north-western side of the Gibel (lee side when looking at the Glacier flow direction). They can be grouped into three clusters as shown in Figure 5. All three clusters clearly are linked to geological faults. The erosional state of the potholes varies between potholes with only a small part of the wall still visible to little sidewall erosion or collapse as seen in Figure 6. Therefore, consistent size measurements of all potholes are not possible. All potholes found are partly filled with sediments. The largest scour form found was in cluster A. It is a curved wall of approximately 10 m in height and 20 m in width on the orographic right side of pothole 1. The smallest pothole was found in cluster C with an approximate diameter of 2 m. Scour forms in cluster B are the least well preserved. This is seen in Figure 6 in forms of cracks (6.3) in the wall and rock break off (6.2). Image 6.4 in Figure 4 shows an over eroded scour form in cluster B. The three closely inspected potholes lie in cluster A and are marked on Figure 5 in red. The measurements of the three potholes are listed below in Table 3.



Figure 6: Top (6.1) and front (6.2) view of a scour form at cluster B with visible wall collapse. The blue line indicates the top edge of the scour form. 6.3 scour form at cluster B. 6.4 over eroded scour form at cluster B.

4.1.1 Pothole 1

Pothole 1 is located at the lower end of cluster A. It is in the part of cluster a where scour forms formed closer together and represents the start of a cascade of scour forms. Pothole 3 lies orographically (when looking at the past glacial flow) to the upper left and to the left is a further smaller pothole. To the orographically right side of pothole 1 the largest scour form of the region is located.

Pothole 1 has a clear elliptical shape. The wavy form of the of the pothole walls in the back part indicates multiple smaller potholes (black circles in Fig. 7). With a major axis of 15 m and a minor axis of 10 m (Fig. 3) pothole 1 is the largest intact pothole found on the Gibel. It is filled with sediments. The wall above the sediment filling of the pothole has a maximum height of 4.5 m. With percussion probing a maximum sediment depth of 3.4 m was determined before hitting hard rock (Point 1 Fig. 7). A second borehole reached 2.2 m (Point 2 Fig. 7). The other boreholes reached all a depth of approximately 1m until hitting hard rock or less when a tree root was in the way.

The maximum depth (H) amounts to 8 m and is calculated from the maximum depth of the sediment filling and the wall height above. The pothole diameter (D) of 12.5m was by taking the mean of the major axis and minor axis. The D/H ratio is therefore 1.56.

Smooth fluvial erosion forms are mainly found in the upper part of the pothole walls. The back wall of the pothole is divided by a horizontal crack (Fig. 8 yellow line). Above the crack the wall shows smooth fluvial erosion. Below this crack, erosion in form of smaller cracks and stone break off are dominant. The horizontal crack dividing the back wall continues into the orographic right-side wall up until the middle where it merges into an approximately 75 cm vertical crack up to the pothole edge. The transition of the back wall into the right wall is marked by a concave wall part. The concave wall part is 60 cm less height than the back wall itself. The front part of the right wall of the pothole can be divided into an upper and a lower part (Fig. 9). The upper part is vertical, smooth and has not that many cracks and rock brake off. The lower part has at the front a strong overhang which evens out toward the back part of the pothole. The overhang is marked by erosion in forms of cracks and rock brake off. The transition of the back wall to the left wall of the pothole is marked by a craggy convex

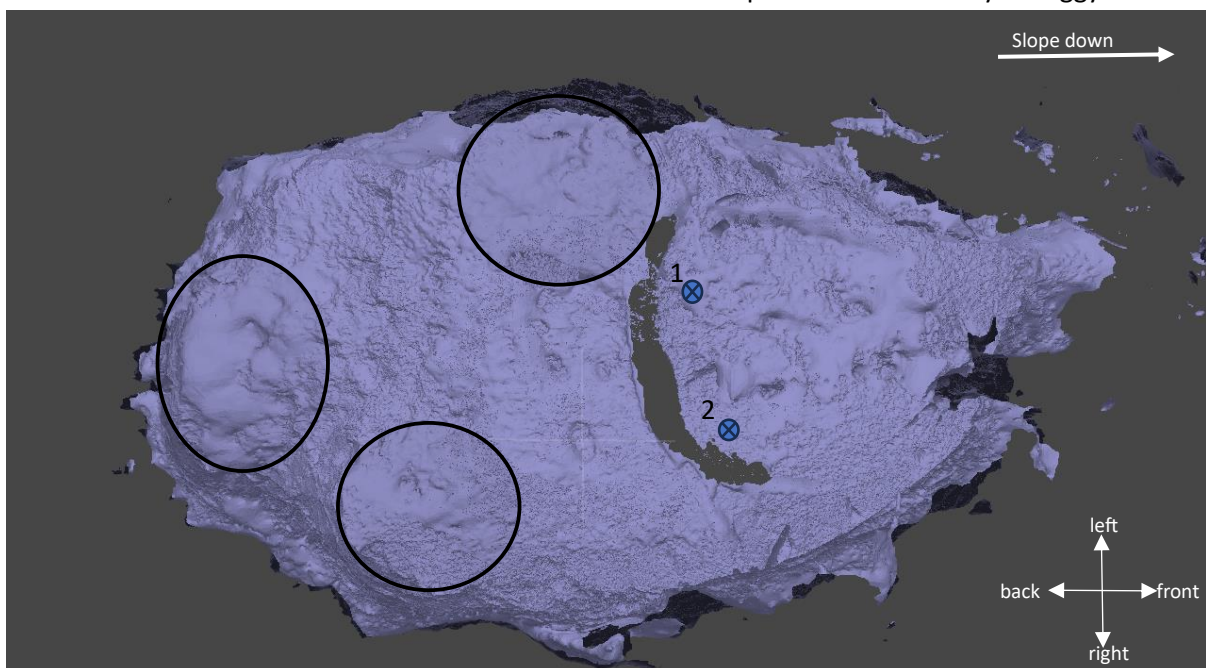


Figure 7: Solid photogrammetric model of pothole 1 with sub potholes indicated (black circles) front of the pothole to the left.

wall part leading into a small overhang in the lower back part of the left wall. The left side wall of the pothole is in general the least smooth wall showing more erosion after the pothole formation. In the front part of the left side, the wall is covered by vegetation. The upper edge of the pothole is not clearly visible on the left side due to vegetation and the steepness of the rock and soil above.

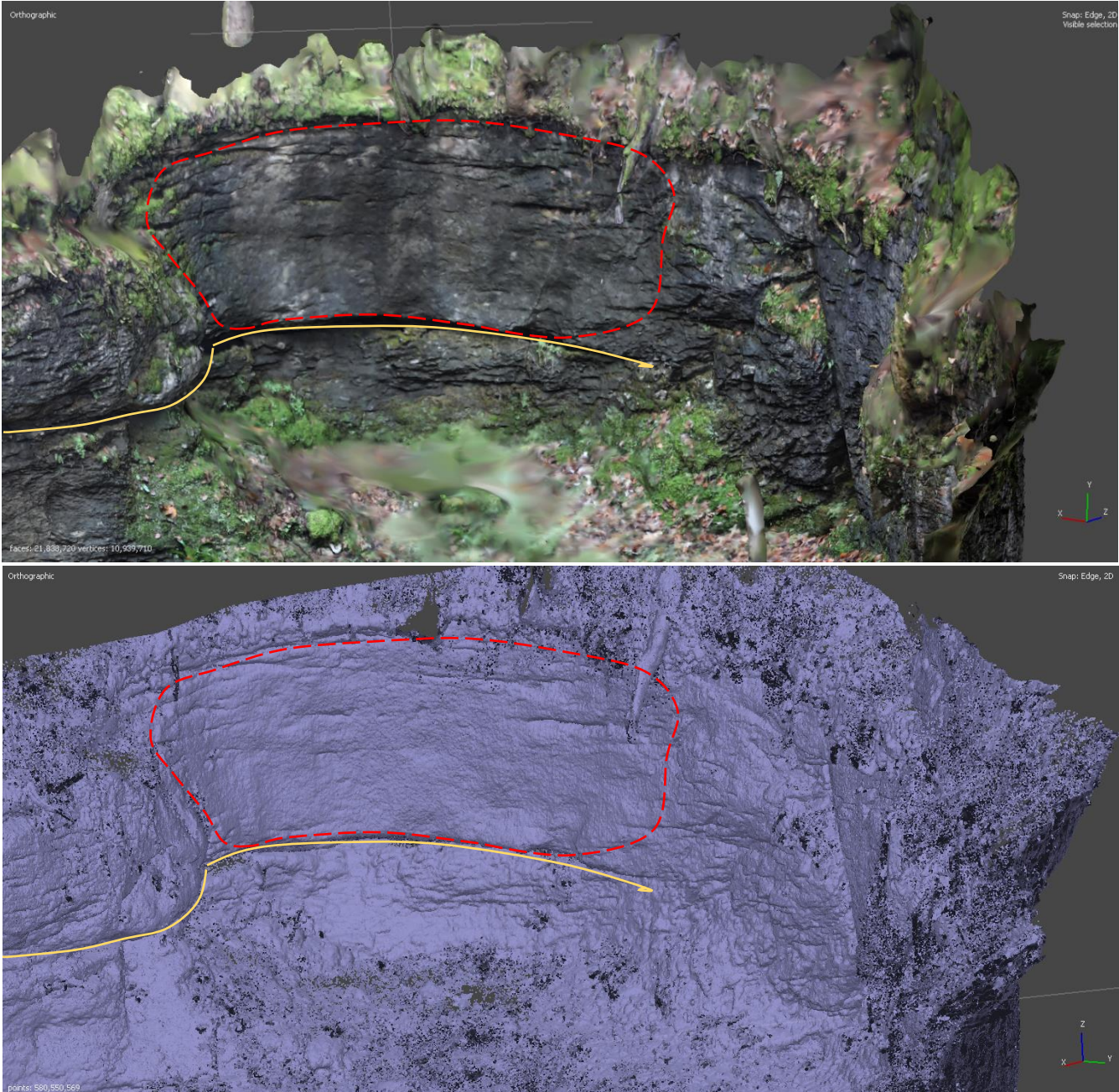


Figure 8: Photogrammetric model of the back wall of pothole 1. Colour shaded (top), nonshaded (bottom). Red dashed line indicates the area of smooth fluvial erosion. Yellow line indicates a crack.

4.1.1.1 Sediment filling

The sediment filling in the front and middle part of the pothole is relatively flat. On the surface some rocks are found. The back part is elevated compared to the rest and the density of rocks found there increases.

The upper most horizon of the sediment filling is 20 cm thick and consists out of humus with a lot of organic matter especially in the top part. The following horizons are from fine (clayey silt) to relatively coarse material (gravel) (Fig. 10). Borehole 1 was filled with water up to a depth of 220 cm. In hole 2 a rise of the water table from 200 cm to 180 cm beneath the surface was measured. The stones found in the lower part of the sediment filling show indication of glacial abrasion with scratch marks and rounded edges. Tabel 2 gives an overview over all the found horizons with the according depth.

Table 2: Soil profile form bore core 1

Depth	Soil description
0 to 20 cm	Humus, earth-moist, lots of foliage
20 to 60 cm	Clayey silt with some gravel (rounded edges), little organic matter, earth-moist, beige grey, loose packing
60 to 80 cm	Clean clay, earth-moist, beige, soft consistency
80 to 110 cm	silty clay with little organic matter, earth-moist, beige, soft consistency
110 to 300 cm	Clayey-silty sand with gravel (rounded edges), earth-moist to 200 cm then wet, grey, loose to medium density packing
300 to 330 cm	Silty-clayey sand with some gravel (rounded edges), wet, grey, loose packing (soft consistency)
330 to 340 cm	Clean gravel (rounded edges), wet, grey, loose packing
>340 cm	Rock or bed rock



Figure 9: Photogrammetric model of the left sidewall of pothole 1



Figure 10: Right picture: Top 80cm of bore core 1 (left), empty bore core (right). Left picture: Bore cores of bore hole 1, depth increases from right to left.

4.1.2 Pothole 2

The second largest pothole which was more closely inspected is further up in cluster A (see Fig. 5). This part of cluster A is less densely packed with potholes than the lower part of the cluster. Pothole 2 has a diameter of 6.5m and is nearly circular in shape. Hand drilling into the sediment revealed a similar composition to the upper horizons of the sediment filling as in the pothole 1. The drilling reached a depth of approximately 90 cm. The maximum wall height above the sediment is 2.7 m. Thus, the pothole has a maximum depth of 3.6m and a D/h ratio of 1.8.

The back wall is an overhang reaching approximately 1.2 m into the pothole at the top (Fig. 11). The overhang lessens over the right side to the front while on the left side it goes over into a vertical wall halfway to the front of the pothole. The front wall is not visible due to soil cover and overgrowth by trees. There is a nearly vertical crack in the back wall. At the top of this crack the edge of the pothole is lowered. To the right the edge is relatively sharp while to the left of the crack the pothole edge is less defined due to later erosion.

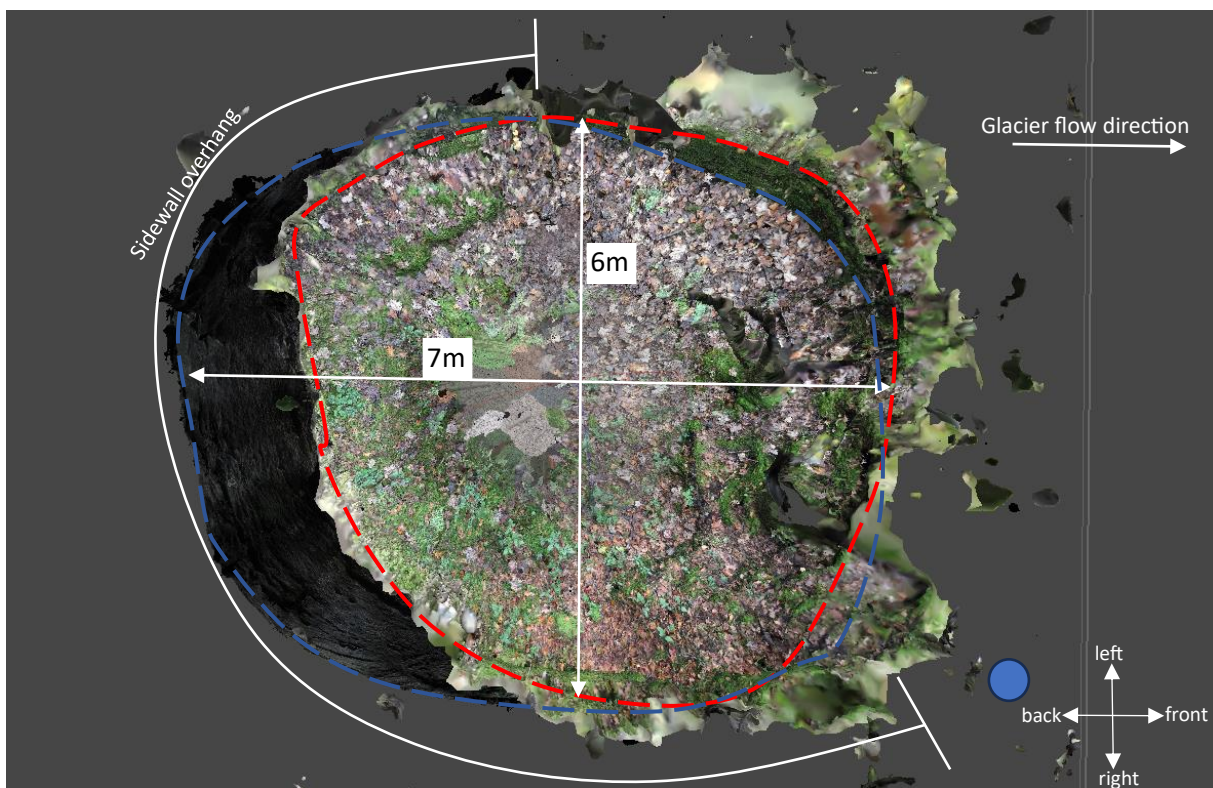


Figure 11: Top view of 3D-model of pothole 2. The frontside of the pothole is to the right. The red dashed line indicates the circumference at the top of the pothole. The blue dashed line indicates the circumference at the height of the sediment filling. The blue dot is the view point of Figure 13.

4.1.3 Pothole 3

Pothole 3 is the smallest of the closely inspected potholes. Located right beside pothole 1 it is also in the lower part of cluster A. It features a major axis of 5.5 m and a minor axis of 3.5 m to 4 m depending on the chosen edge of the pothole. It is filled with 30 cm of soil and has a wall height of 2.3 m. Thus, the D/h ratio is 1.9.

The distinguishing feature about pothole 3 is the rock which reaches into the pothole (marked red in Fig. 12). It has a shape of a curved V and the vegetation free surfaces are relatively smooth. The walls of the pothole are the least well preserved of the 3 closely inspected potholes. Therefore, the original shape of the potholes is not clearly visible.

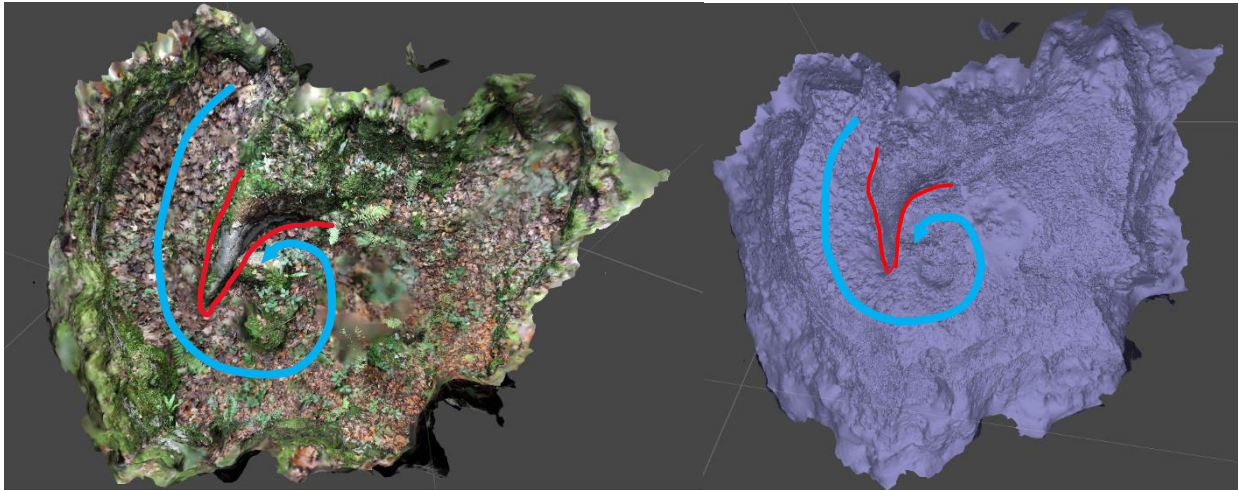


Figure 12: Pothole 3 photogrammetric model top view. Coloured model (right), uncoloured model (left). Blue line indicates the flow direction of the water.

Table 3: Pothole measurements

	Pothole 1	Pothole 2	Pothole 3
Major axis (m)	15	7	5
Minor axis (m)	10	6	3.5-4
Height above soil (m)	4-6	2.7	2.3
Soil depth (m)	3.4	0.9	0.3
Diameter/Height	1.5625	1.805	1.9

4.2 Discussion

In the first part of this section, it will be discussed why the erosion forms on the Gibel are potholes and not sinkholes. Then a closer look will be taken at accuracy of the 3D scans/models of the potholes.

4.2.1 Sinkhole vs Pothole

In karstic regions hole like features are a common site in the form of sinkholes. These forms due to the subsurface erosion and chemical removal of limestone, which leads to the formation of caves and later to the collapse of the cave roof to form a sinkhole (Baryakh and Fedoseev, 2011). The collapse of sinkholes leaves behind a craggy wall. When looking at the walls of the potholes on the Gibel as described in the section above, they appear smooth with a rounded shape, which indicates to a fluvial nature of the erosion. The rock reaching into pothole 3 (red marking in Fig. 12) further strengthens this conclusion. With its rounded form it further indicates the flow direction of the water during pothole formation. Water was flowing in along the narrow channel between the rock and the

pothole wall. The vortex was located on the other side of the rock giving it the distinct curved shape. However, this does not mean that the erosion found in the potholes is only fluvial in nature. Parts of the pothole walls eroded further after the pothole formation indicated by the craggy wall parts as seen when looking at overhang in the lower part of the right sidewall of pothole 1 (Fig. 9), the vertical crack in the back wall of pothole 2 (Fig. 13) or most of the side wall of pothole 3.

4.2.2 Pothole evolution

The general shape of the pothole can give an indication of the evolutionary state of the potholes when the initial fluvial erosion stopped. The three closely inspected potholes have all different shapes. Pothole 1 is elliptical and the wavy walls indicate multiple potholes (see black circles in Fig. 7). The coalescence of potholes occurs most often during the late stages of pothole evolution (Lorenc, Barco and Saavedra, 1994; Das, 2022). The overhanging back wall of pothole 2 indicates that it is in a similar or slightly younger evolutionary state as pothole 1. The lack of multiple potholes growing into pothole 2 can be explained due to its relative isolation. Pothole 3 is the least evolved pothole of the closely inspected ones. This statement is based on the least over eroded parts of the wall and the rock reaching into pothole 3.

Ji, Li and Zeng (2018) found that the diameter to depth ratio (D/H) can give an indication on the pothole's grinder size. The D/H ratio of the closely inspected potholes lies somewhere between the ratio found by Ji, Li and Zeng (2018) of 1.56 and 2.2 for marine and hillside potholes respectively. This indicates a grinder size between sand and cobbles. Here it has to be stated that the D/H for the closely inspected potholes has some uncertainty to it. The uncertainty is due to the method the pothole depths were measured. The maximum depth of the sediment filling was found by drilling into it. When hitting a large rock or a tree root, the drill could not overcome the obstacle and advance further even though the pothole might be deeper.

4.2.3 Sediment filling

The sediment fillings of the potholes consist of a 20 cm humus horizon followed by sorted nonorganic sediment where the finest clay is found near the top and sand and bigger pebbles follow further down. This indicates that the pothole started to fill with sediments during or right after the glaciation when there was still a flow of water into the pothole. However, the waterflow was not strong enough to erode the pothole further. This finding gets furthermore supported by the small pebbles with scratch marks found in the lower parts of the sediments. The potholes lie in a karst area with no surface discharge to transport sediments into the potholes. Hence, significant sedimentary filling most likely stopped relatively short after deglaciation.

The potholes are not filled with water even after a rain event. However, in the two deep boreholes water was infiltrating through the soil filling up the holes to a certain height. This leads to the conclusion that there must be subsurface drainage of water out of the potholes. Because they are located on top of a hill, there is only a very small area from which non glacial sediments could originate.

The bigger rocks found on the surface of the sediment filling and in the back of pothole 1 tend to have sharper edges and no scratch marks. Due to that they most likely come from the partial collapse of the side walls. Especially the higher sediment filling in the back which lies directly beneath the craggy overhang found in the back part of the right-side sidewall.



Figure 13: Backwall of pothole 2. The red and blue dashed lines indicate the top and bottom edge as in Figure 11

5 Model work

5.1 Results

This section of the thesis covers the results of various IGM (Jouvet *et al.*, 2021) model runs over the Reuss-Muotatal area. The model runs were conducted using two different resolutions (200 m and 100 m) with different fixed ELA's. Furthermore, a 200 m resolution run was calculated using the EPICA climate for the Alpine region.

5.1.1 Ice extent and thickness

The extent of the modelled glaciated area depends on the chosen ELA height as seen in Figure 14. A lower ELA corresponds to a larger area of glaciation. The modelled glacier extent exceeds the model area completely at an ELA of 1300 m a.s.l. Furthermore, Figure 14 shows that the Gibel is glacier covered for each model run up to an ELA of at least 1700 m a.s.l.

When looking at the thickness it can be observed that the modelled glacier is thickest in the deep valleys and less thick on the mountain tops. Furthermore, the overall thickness decreases with a higher ELA as seen for example on the north part of the Rigi. In the 1300 m and 1400 m ELA runs the whole Rigi north side is covered with ice while in the 1460 m to 1500 m ELA runs the ice reaches a height from 1080 m to 940 m respectively. This corresponds to an ice thickness of 370 m to 230 m respectively. Looking at the Gibel it can be observed that the ice thickness also varied between the different model runs. A higher ELA corresponds to a thinner glacier. The thickness of the ice over the area of cluster A is at its maximum thickness 1375 m (ELA 1300 m a.s.l.). This corresponds to an ice surface height of 2125 m a.s.l.

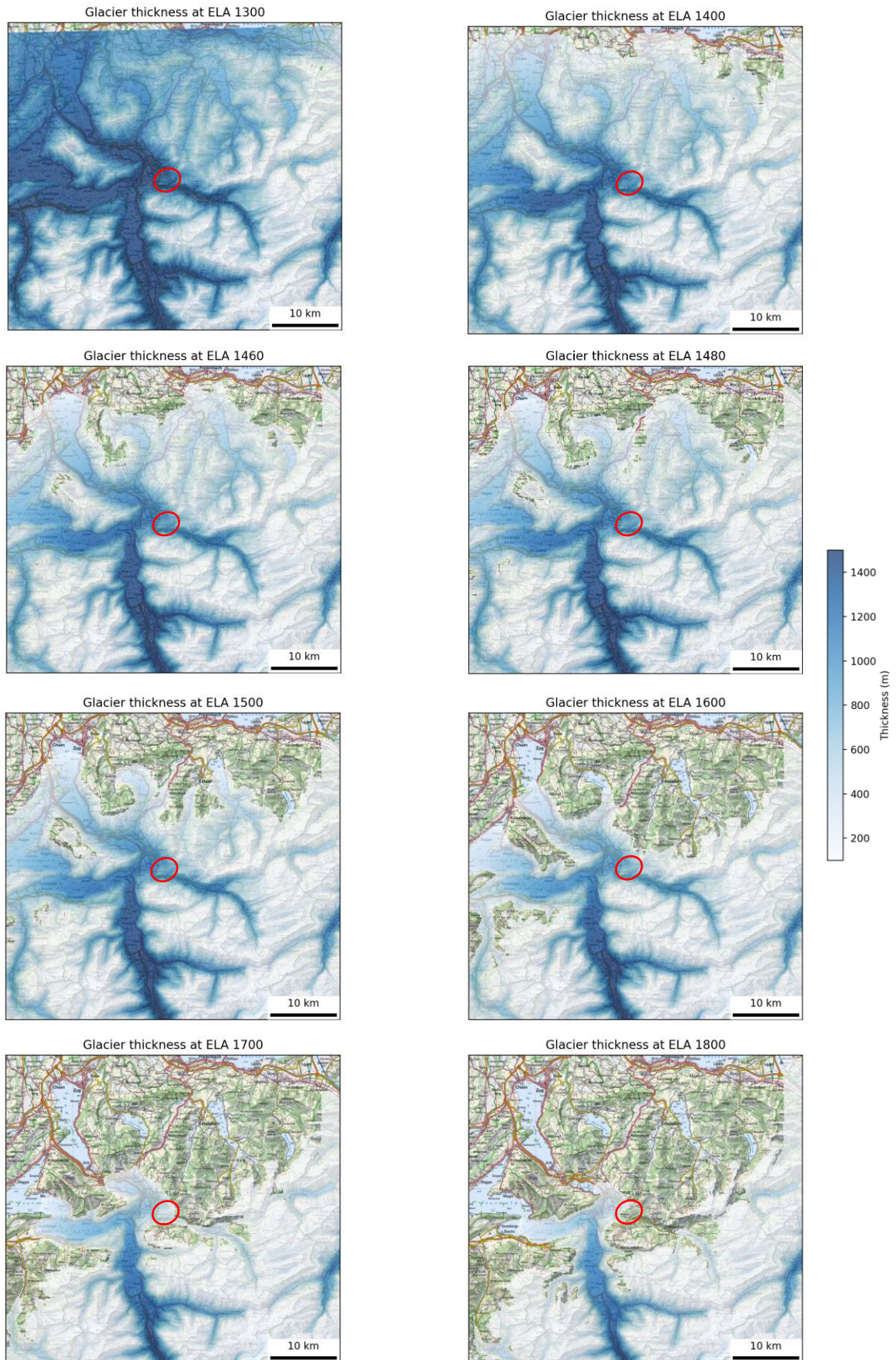


Figure 14: Thickness of the Reuss and Muota glaciers after 5000-year advance model run with a fixed ELA at a resolution of 200 m. The red circle annotates the Gibel.

5.1.2 Ice surface Velocity

As seen in Figure 15 the highest surface velocities are modelled over the Reuss valley. Looking at the Muota valley a higher speed compared to the surrounding area is seen except at an ELA of 1300 m a.s.l. At this ELA the modelled surface ice flow in the whole lower Muota valley and the following Lauerzersee region decreases. Simultaneously, an increase in the surface flow velocity the Alphal and the Ibrig region is seen. For the ELA's 1400 m to 1600 m a.s.l. the model shows a decrease in speed and widening of the area with higher speed over the Gibel. The highest ice velocity over the Gibel is modelled over the area of the pothole clusters A and B. At the ELA's 1700 m and 1800 m a.s.l. the Gibel starts to be located close respectively at the ice margin and the higher surface ice speed shifted from the Gibel into the Muotaschlucht.

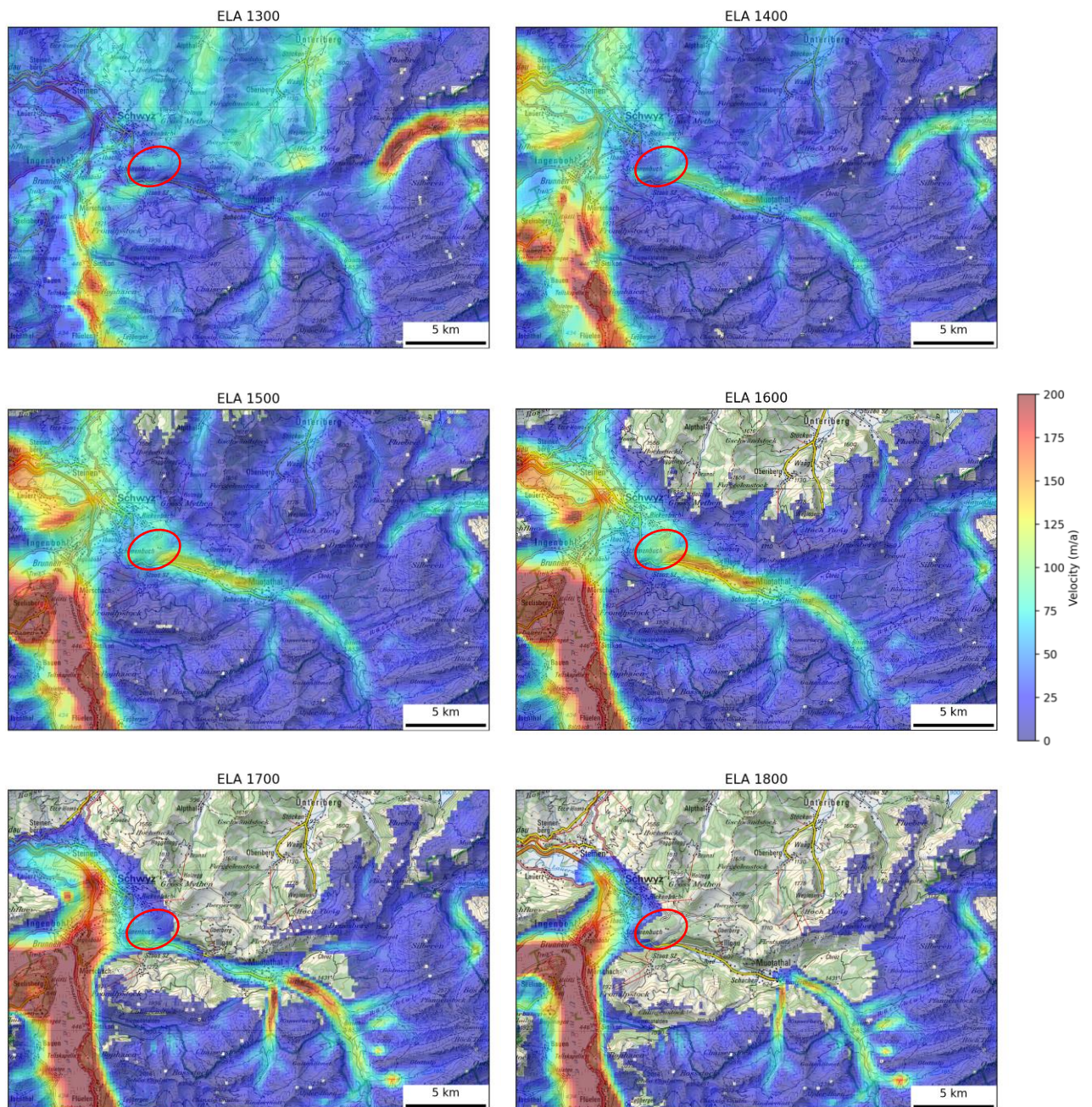


Figure 15: Modelled surface ice velocity of the Muotathal area with different ELA heights at a resolution of 200 m.

5.1.3 Flow direction and sediment transport

To get a better understanding where the pothole filling came from and why the potholes are not completely filled with sediments as it was the case in Lurcer (Keller, 2021), ice flow lines were calculated using the modelled surface movement (Fig. 16). Assuming the different ELA steady states are a good approximation of how the Reuss-Muota glacier looked during the end of the LGM it is apparent that ice overflowing the Gibel came from different regions during different times. At the start of the glacier retreat ice overflowing the Gibel came out of the Chaiserstock region and later the Muota valley corresponding to the ELA's 1400m up to 1600m a.s.l. in Figure 16. During later stages the Muota glacier retreated further and the ice from the Reuss glacier flowed up the Muotaschlucht and over the Gibel (corresponding to ELA's 1700m and 1800m a.s.l.). At these ELA's the ice reaching the Gibel originates in the Klausenpass region.

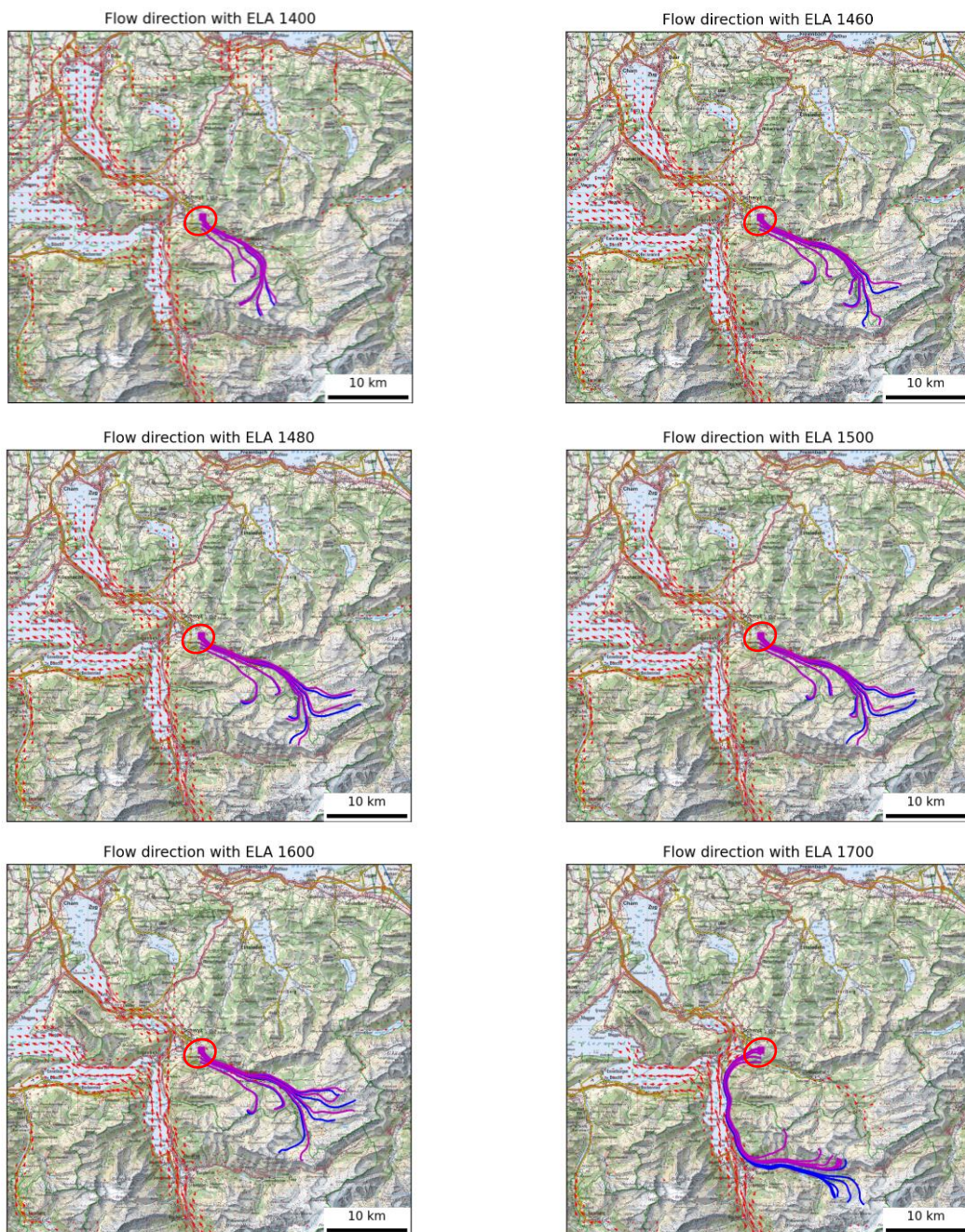


Figure 16: Thickness of the Reuss and Muota glaciers after 5000-year advance model run with a fixed ELA and a resolution of 200 m. The red circle annotates the Gibel.

5.1.4 Strain rate

The strain rate gives an indication to where crevasses form on a glacier. Crevasses act as a way for water to infiltrate the glacier from the surface to the glacier bed (Hooke, 1991; Alley, Cuffey and Zoet, 2019). This happens by the filling of the crevasse with melt water what can lead to the formation of moulines (Holmlund, 1988). These moulines are kept open by the friction melting of the water flowing through them (Holmlund, 1988) towards the glacier bed (Alley, Cuffey and Zoet, 2019). In Figure 17 the maximum strain rate over the Muotathal region is shown. The highest strain rates in the Muota valley are modelled over the north side of the valley. The model also shows a local strain rate maxima right above the Gibel and a strain rate of 0.05 a^{-1} over the clusters A and B for ELA's between 1400m a.s.l. and 1600m a.s.l. Therefore, it can be assumed that the region in front and over the Gibel were a source of surface melt water for subglacial water system.

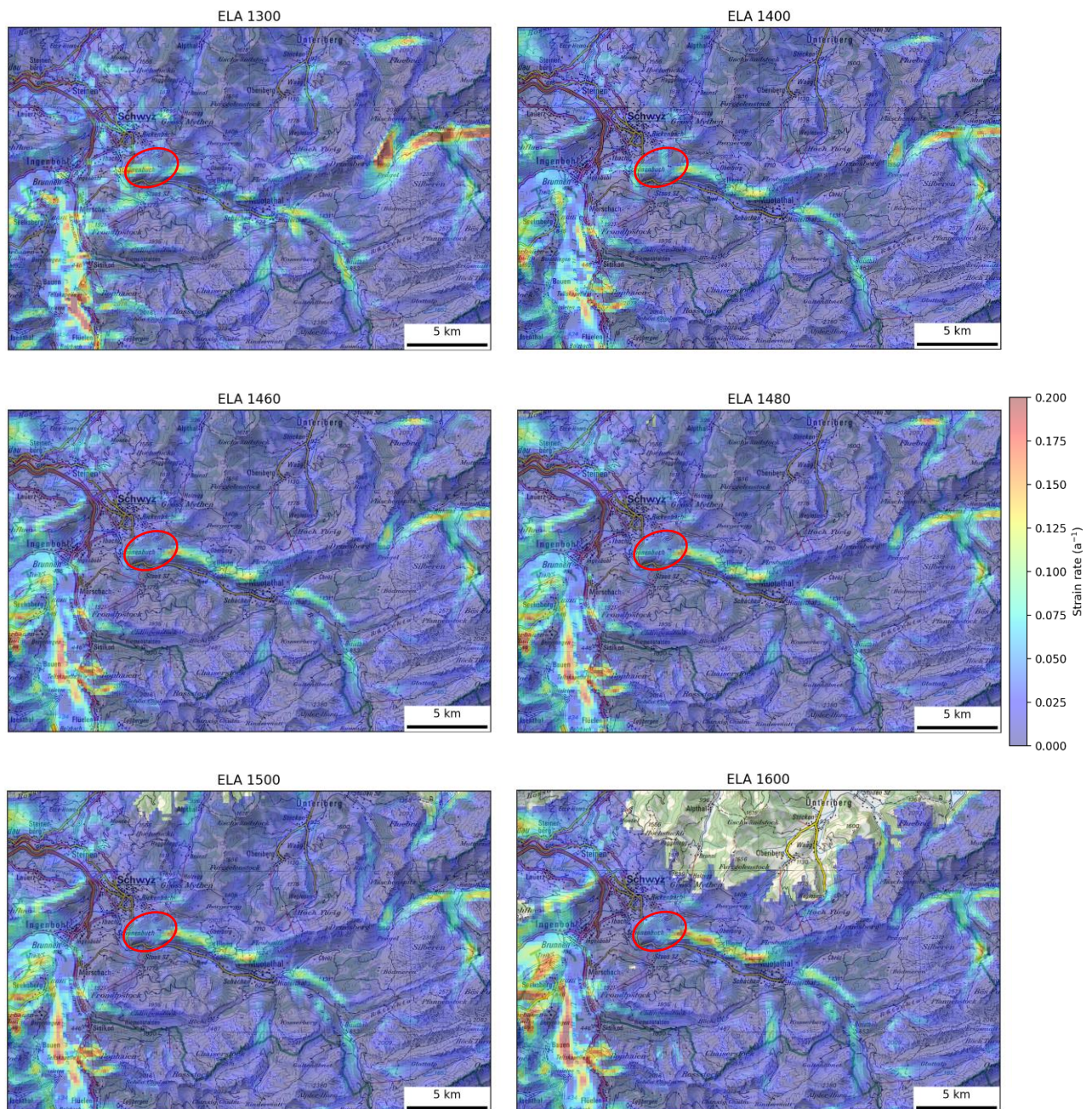


Figure 17: Modelled maximum surface strain rate in the Muotathal region with different ELA heights at a resolution of 200 m.

5.1.5 Hydraulic potential

The formation of potholes is directly connected to the flow of subglacial water. Figure 18 shows water pathways over the glacier bed based on the hydraulic potential calculated using the modelled glacier surface at a model resolution of 200m. These modelled water pathways indicate the subglacial water channels. When looking at the Gibel, water channels overflowing it are indicated for the ELA's of 1460 m, 1480 m and 1500 m a.s.l. However, the area which drains over the Gibel varies between the whole upper Muota valley at ELA's 1460 m and 1480 m a.s.l. and just relatively locally at the ELA of 1500m a.s.l. The model runs with an ELA of 1700m and 1800m a.s.l. are showing water flow over the Gibel coming from the whole Muota valley. However, it has to be mentioned that the flowline calculations assume a lake in the Muota valley dammed by the Reuss glacier (Fig. 22). Looking at different time steps at the end of the modelled time span (assumed steady state) the flowlines over the Gibel do not change for the 200m resolution runs.

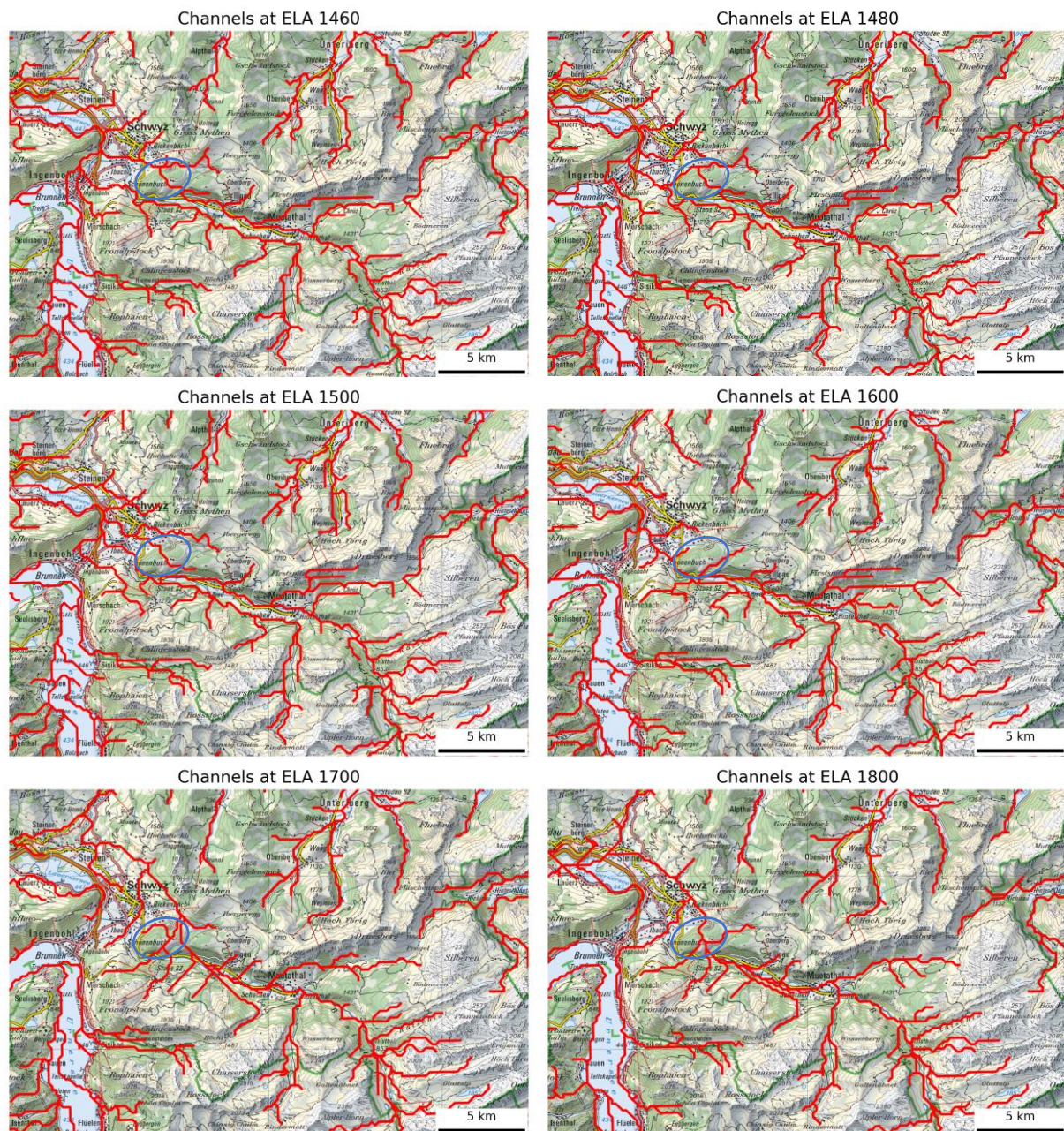


Figure 18: Subglacial water pathways (red) based on the hydraulic potential at the glacier bed calculated using the fixed ELA model runs 200 m resolution. The blue circle marks the Gibel.

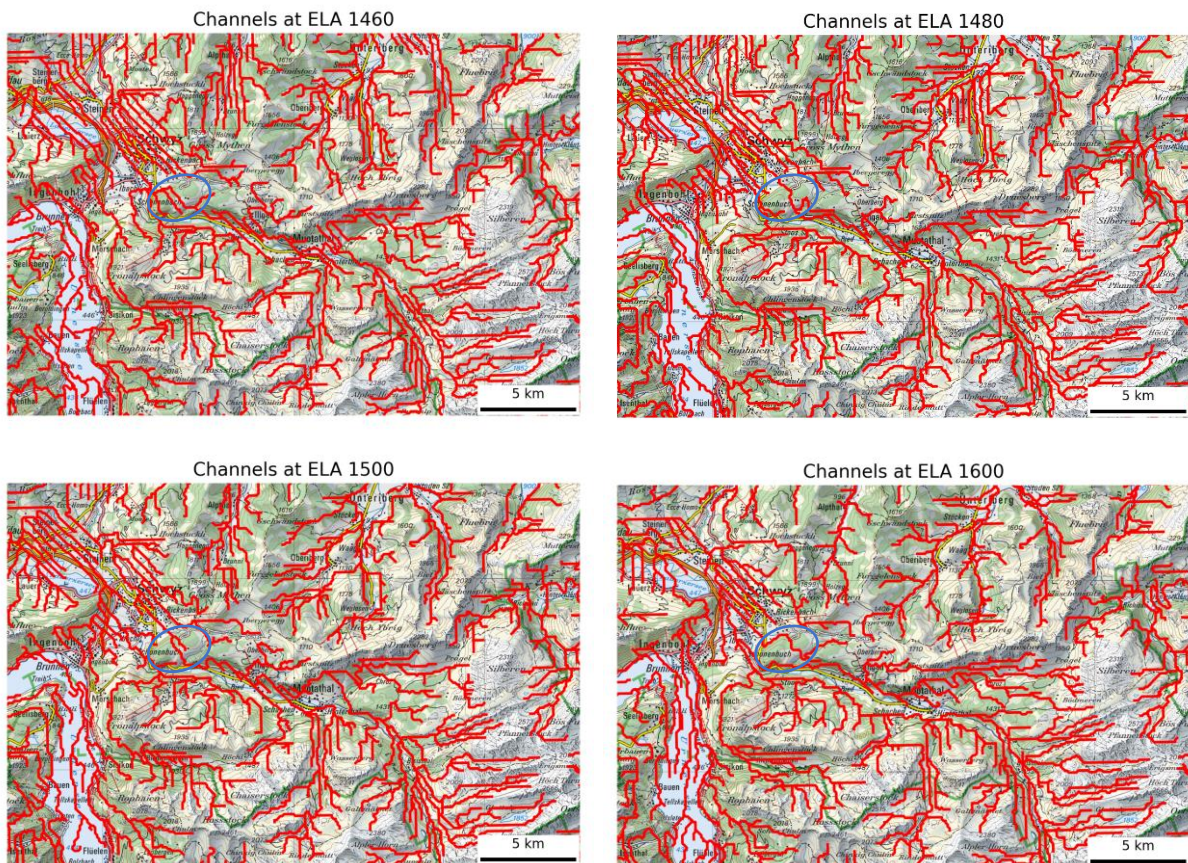
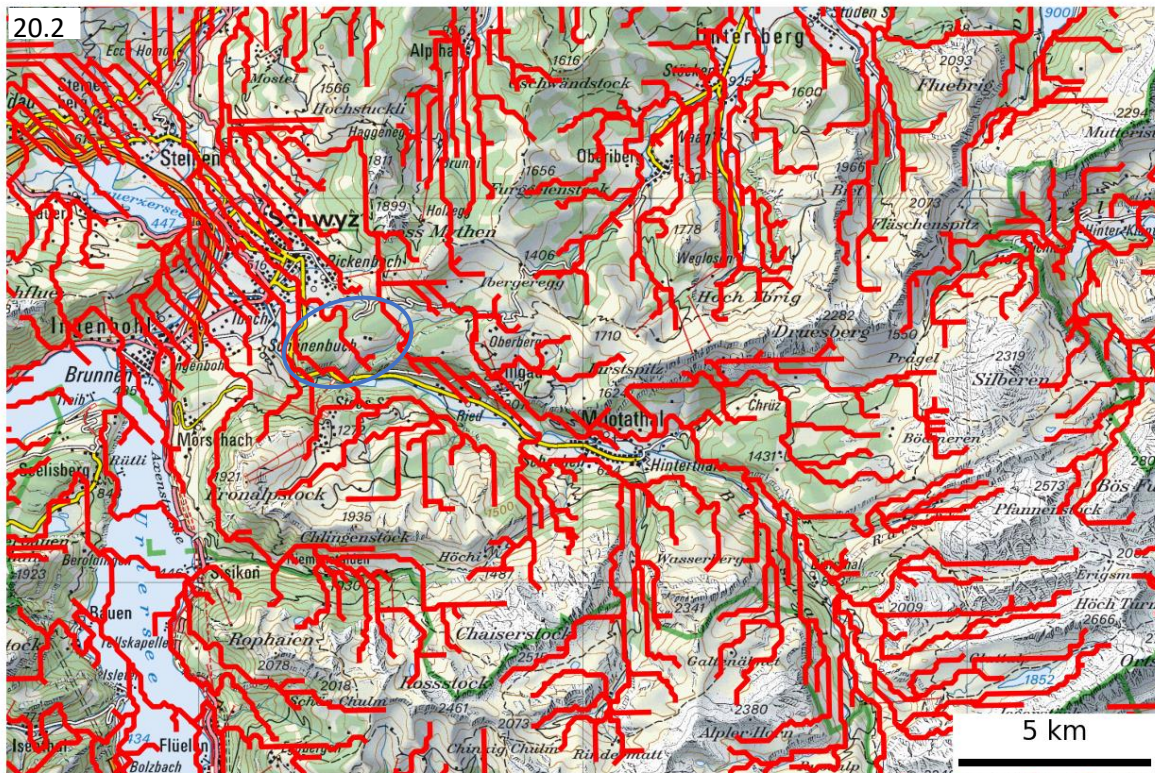


Figure 19: Subglacial water pathways (red) based on the hydraulic potential at the glacier bed calculated using the fixed ELA model runs 100 m resolution. The blue circle marks the Gibel.

This changes when looking at the 100m resolution model runs (Fig. 19). These run show overall similar results to the 200m. However, when looking at different time steps during the assumed steady state movement of the water pathways over the Gibel can be observed (Fig. 20). While the water pathways still indicate flow over the Gibel the significant difference is in the catchment area of those potential subglacial streams. In Figure 20.1 the Muota valley is drained over the east side of the Gibel (pothole cluster C) while 500 years later in Figure 20.2 the Muota valley drains over the middle of the Gibel where the pothole cluster A is located. The subglacial catchment area draining over the cluster A therefore changes from 193 km² to 2 km².

Channels at ELA 1460 after 9500 years



Channels at ELA 1460 after 10000 years

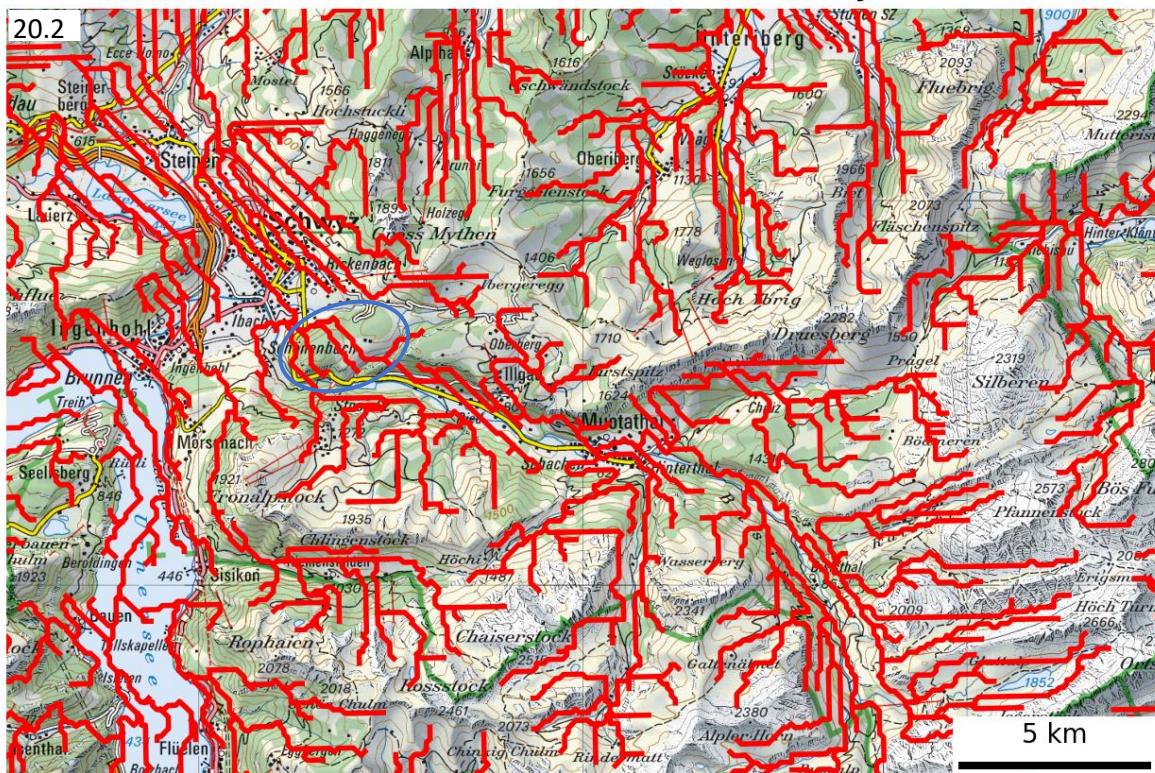


Figure 20: Subglacial water pathways (red lines) based on the hydraulic potential calculated using the 1460 m a.s.l. ELA 100 m resolution IGM run at two different times. The blue circle marks the Gibel.

5.1.6 EPICA Run

The first EPICA model run was conducted over time span between 35000 BP to 10000 BP with a current day ELA of 3000m a.s.l. During this period the model shows that the Gibel was ice covered for 19400 years between 34600 BP to 15000 BP. The maximum glacier extent exceeds the modelled area. The ice thickness over the Gibel changed suddenly from 1000 m during the first 2000 years of glaciation to about 1300 m until deglaciation starts (Fig. 21.1). The model run with a current day ELA of 3250 m a.s.l. has a similar sudden increase in thickness, especially seen on the Stoos and Rigi at 26 ka BP (Fig. 21.2). This increase in thickness also occurs shortly after the glacier exceeds the model area. While the runs with a current day ELA of 3000 m and 3250 m a.s.l. exceeded the model area during the LGM the 3350 m current day ELA run (Fig. 21.3) only reached a few kilometres farther than Zug. The water pathways calculated show that water was flowing over the Gibel during multiple stages of maximum glaciation with all three ELA heights. Furthermore, during the retreat water pathways in all three models run indicate channels which are draining the upper Muota valley flowing over the Gibel (similar to Fig. 17 ELA 1480).

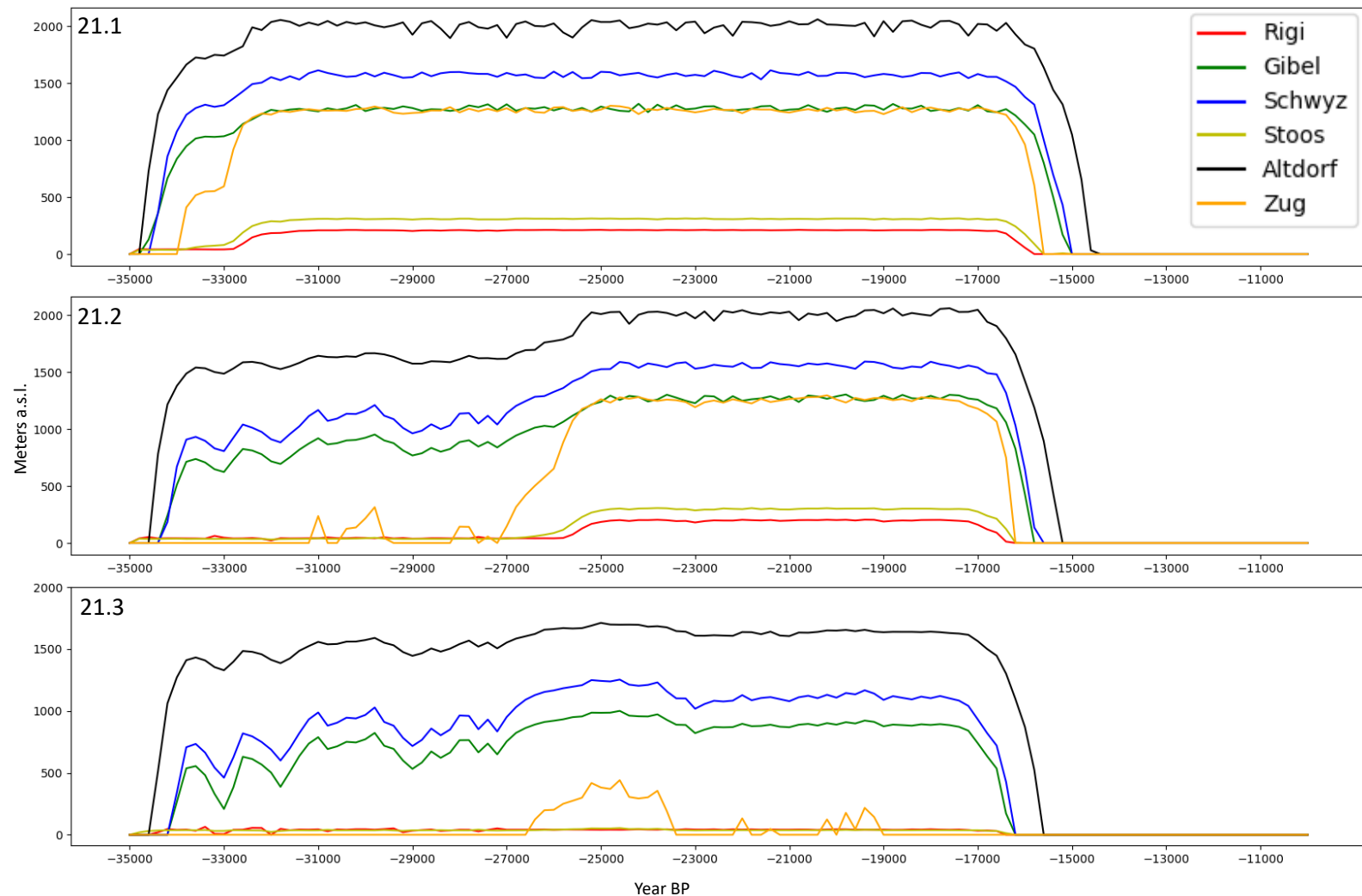


Figure 21: Ice thickness at different points in the study area during EPICA model runs using a current day ELA of 21.1) 3000 m a.s.l., 21.2) 3250 m a.s.l. and 21.3) 3350 m a.s.l.

5.2 Discussion

The goal of modelling the Reuss-Muota glacier was to get a better understanding of condition which led to the formation of the potholes on the Gibel. This part of the thesis takes a critical look at the model results presented above.

5.2.1 Subglacial Waterflow

The hydraulic potential was used to get a first understanding of the subglacial water channels under the glaciers and water streams around the modelled glacier. As already indicated by the potholes found on the Gibel, the flow lines show water flow over the Gibel during certain stages of the glaciation for the fixed ELA runs and the EPICA runs. Furthermore, these water pathways are stable over multiple timesteps in the 200m resolution runs. While for the 100m resolution runs the catchment area differs there is still predicted flow over the Gibel over multiple timesteps. It must be noted however, these water pathways do not consider where surface water is reaching the glacier bed. The strain rate is therefore used to get a knowledge of areas of crevassing which can act as conduits for surface water to reach the bed (Hooke, 1991). The location of a higher strain rate area before the Gibel is seen over the ELA's 1400 m a.s.l. to 1600 m a.s.l. (Fig. 17). This is an indication that even if the basal water of the Muota valley discharged through the Muotaschlucht that surface melt water reached the pothole areas.

5.2.2 Muota valley Lake

For the water pathway calculations of the model runs ELA 1700m a.s.l. and 1800m a.s.l. it was assumed that the Reuss-glacier dammed the Muota valley in the Muotaschlucht. Therefore, a lake would have been formed in the Muota valley (Fig. 22). The formed lake of the ELA 1800m run drains over the pothole cluster A. (sediment load out of a lake small). Lake sediments are found in the Muota valley by Hantke, Pfiffner and Gouffon (2013). However, they conclude that these sediments come from flat lakes dammed by debris flow not indicating a lake filling the whole Muota valley. However, similar lakes are found today for example in the Tien Chen mountains (Merzbacher lake) (Kingslake and Ng, 2013) and Alaska (Berg Lake) (Dilles *et al.*, 2019).

5.2.3 Sub- and Supraglacial sediments

The erosion of bedrock potholes can only occur when there is no protective sediment layer over the bedrock, but enough sediment suspended in the water for abrasion to occur (Hancock, Anderson and Whipple, 1998). The main driver of subglacial sediment removal is thought to be subglacial R-channels feed by meltwater from the surface through moulins and crevasses (Hooke, 1991; Creyts, Clarke and Church, 2013). The modelled high maximum strain rate in front of the Gibel (Fig. 17) therefore acts as the water source for the channels assumed to follow the water pathways crossing the Gibel in Figure 18. Secondly the Gibel is like a ridge at the end of an over-deepening. Water coming from the Muota valley decreases in speed when flowing over the Gibel due to a decrease in the gradient of the hydraulic potential. Furthermore, an adverse slope can lead to a shutdown of the efficient R-Channel system (Werder, 2016). Such a shutdown would lead to a sediment deposition in front of the Gibel and therefore less sediments on the Gibel itself.

Another potential reason for the lack of sediments in the potholes is the location from which the glacier ice reached the pothole area. Glacier ice is modelled to reach the Gibel region from the upper Muota valley and the Klausen pass region (Fig. 16). These regions do not have a lot of high rock cliffs producing glacial sediments by rockfalls onto the glacier.

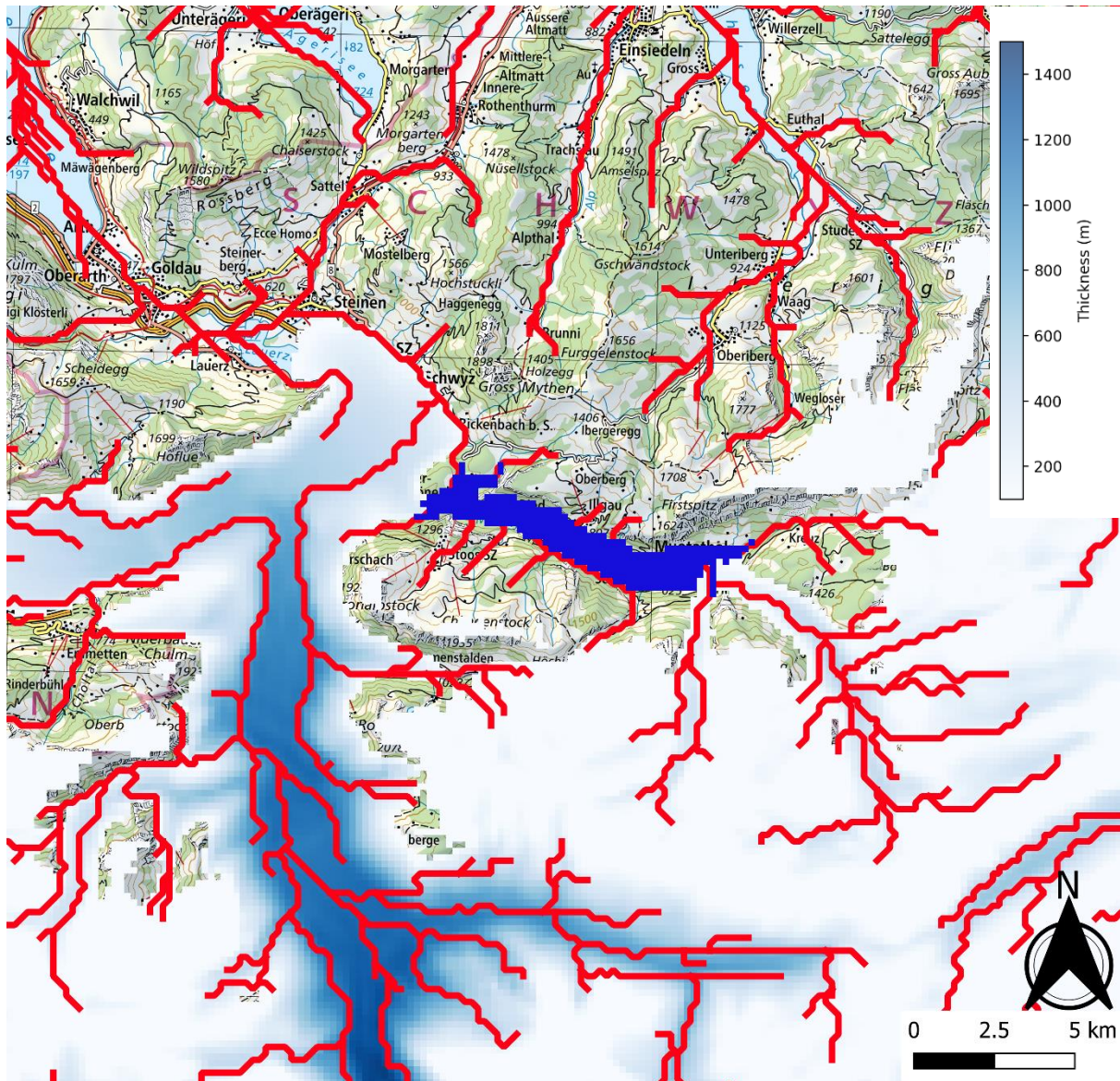


Figure 22: Possible maximum extend of the Muotavalley lake (dark blue) during the glacier retreat after the LGM. The subglacial water pathways (red) and the glacial thickness are shown (ELA 1800).

5.2.4 Comparison to Geomorphological data and other models

Comparing the model results of this study with geomorphological data and models of the Reuss region in other studies, the IGM overestimates the ice thickness. Erratic boulders found by Reber *et al.* (2014) at the Rigi north side result in an ice surface height during the LGM of approximately 1000m a.s.l. The fixed ELA runs up to 1450m a.s.l. result in a similar ice height for this region for a glacier extent 30 km shorter than the LGM. Looking at the EPICA run with a current day ELA of 3000m a.s.l., the ice thickness over the Gibel at the LGM is 850m higher as the map of Bini *et al.* (2009), which uses trimlines as the ice surface height, indicates. The ice surface of the model during the LGM lies approximately at 2100m a.s.l. compared to the approximately 1400m a.s.l. found by Bini *et al.* (2009). The EPICA run with a current day ELA of 3350 m a.s.l. has an ice thickness leading to an ice surface height similar to the trimline height. However, the modelled glacier extent during the LGM

only reaches Zug. Hence, the modelled glacier is 30 km shorter than indicated by the moraines found around Birr. This shows that the IGM using the starting conditions of this thesis models the glacier with a steeper tongue than the geomorphological data suggest. It has to be noted however, trimlines tend to underestimate the glacier height (Cohen *et al.*, 2018; Seguinot *et al.*, 2018). Hantke, Pfiffner and Gouffon (2013, p. 42) describe an ice surface at a maximum height of 760m a.s.l. $19\,185 \pm 245$ BP in the lower Muota valley due to the finding of a bear teeth dated to that time. In contrast to that all EPICA model runs show an ice thickness of over 800m over the Gibel during this time (see Fig. 21).

5.2.5 Model stability and accuracies

When looking more closely at the 100m resolution model results it is apparent that the glacier surface shows a wave pattern especially over the deeper valley sections with thicker ice. An example of this can be seen between Urnersee and the Zugersee (Fig. 23 red circle). These wave patterns have an amplitude of several 100 meters over horizontal distance of 200 m. When comparing these waves to present day large arctic valley glaciers it becomes obvious that such glacier surfaces are not realistic. Furthermore, the wavy surface impacts directly the hydraulic potential since the hydraulic potential is calculated using the glacier surface. This can also be seen in the multiple parallel flow lines over the Schwyz area (Fig. 19). While model stability/accuracy can be increased by lowering the cfl-Number the run duration increases. However, decreasing the cfl-number from 0.05 to 0.01 did not show visible improvement of the model glacier (decrease in waviness of the surface) while increasing the runtime significantly. This hints to other model inaccuracies than just model stability. An other contribution to the model inaccuracy might be the fact that the ice age glacier thickness exceeds the data used to train the neural network the model runs with (f17_cfsflow_GJ_22_a) (Jouvet, 2023).

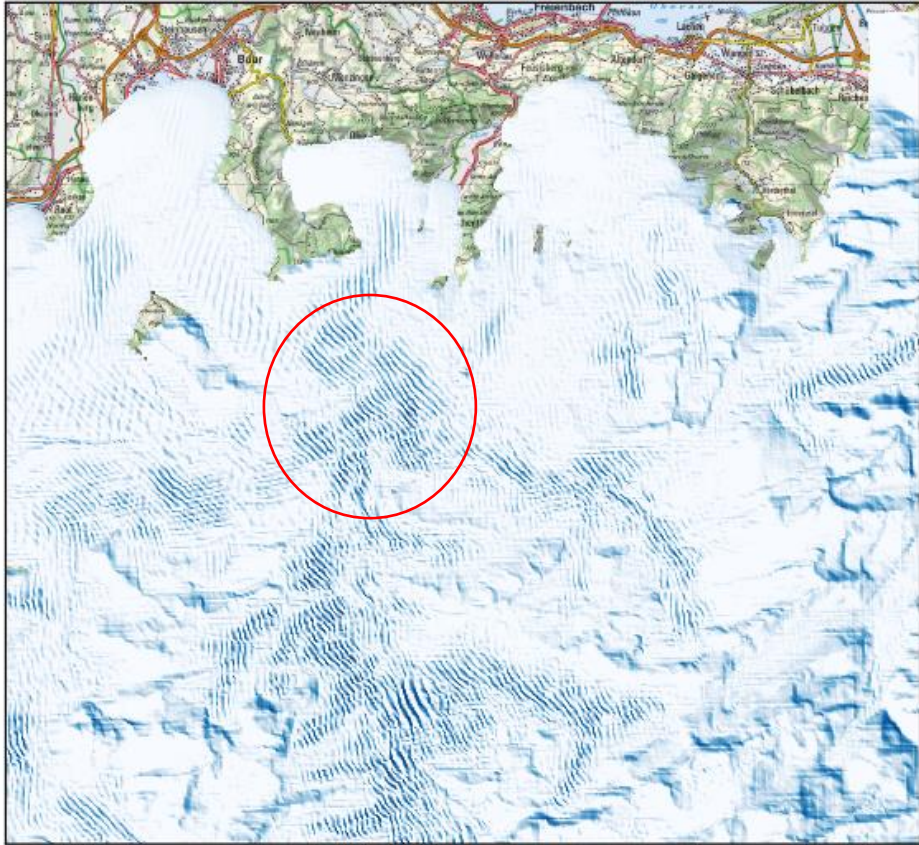


Figure 23: Comparison between model runs at a resolution of 100m (top) and 200m (bottom).

6 Conclusion

The location of the potholes on top the Gibel indicate that water must have flown over the Gibel at some point in time. The karstic nature of the bedrock and resulting lack of surface water discharge, excludes formation due to rivers. The karstic nature of the study area further could lead to the assumption that karstic erosion processes formed these potholes in the same way sinkholes are formed. However, the morphology of the potholes clearly indicates fluvial erosion. Further, the size of the potholes makes a formation due to rain implausible. Hence, glacier and subglacial water come to mind as a formation criterion. This thesis showed through modelling that under the right conditions during the last ice age subglacial water of the Muota valley drained over the Gibel and the pothole clusters. The flow direction of the subglacial water pathways at different ELA's matches the direction of the pothole clusters indicating different formation times for the different clusters. Hereby, already existing faults in the bedrock facilitated vortices to grind out the potholes. Further the model showed even when the subglacial water from the Muota valley drained trough the Muotaschlucht glacial crevasse fields in front of the Gibel could act as a water source for the pothole formation. The partially filling of the potholes with sediments can be explained by the breakdown of the channelised subglacial water system due to a revers slope. A further lack of larger rocks with glacier marks is most likely due to the lack of high rock cliffs in the area of ice origin overflowing the Gibel. While the modelling results give a first clue where the sediments found in the pothole originated further investigations into their chemistry might give a better insight into their origin. Furthermore, the model used in this thesis was only trained up to an ice thickness of 1000 m. Hence, for future modelling of the Alpine glaciers during the last glacial cycle training of the model to ice thickness of 1500 m to 2000 m would be preferable.

7 Acknowledgments

During this master thesis I got helped by lots of people. I would like to thank my supervisors Martin Lüthi for supporting me during the whole process of data collection to thesis writing. Further I would like to thank my second supervisor Lukas Inderbitzin who organized drilling equipment and took a Saturday to get depth measurements in the Potholes. Also, I would like to thank Boris Ouvry for helping me with the cleanup of the LiDAR scans of the potholes. The modelling process would not have been possible without the development work of Guillaume Jouvét and his and Adrien Wehrlé's when I crashed the omen server. For that I would like to thank them. At last, I would like to thank Hans Wehrli and Silvia Juen for proofreading my thesis at the end.

8 Bibliography

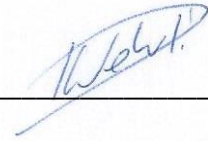
- Alexander, H. S. (1932) 'Pothole Erosion', *The Journal of Geology*, 40(4), pp. 305–337. doi: 10.1086/623954.
- Alley, R. B., Cuffey, K. M. and Zoet, L. K. (2019) 'Glacial erosion: status and outlook', *Annals of Glaciology*, 60(80), pp. 1–13. doi: 10.1017/aog.2019.38.
- Bartos, M. *et al.* (2022) 'mdbartos/pysheds: 0.3.1'. doi: 10.5281/ZENODO.5842711.
- Baryakh, A. A. and Fedoseev, A. K. (2011) 'Sinkhole formation mechanism', *Journal of Mining Science*, 47(4), pp. 404–412. doi: 10.1134/S1062739147040022.

- Bini, A. *et al.* (2009) 'Die Schweiz während des letzteiszeitlichen Maximums (LGM): 1:500 000', *Bundesamt für Landestopografie, swisstopo*.
- Cohen, D. *et al.* (2018) 'Numerical reconstructions of the flow and basal conditions of the Rhine glacier, European Central Alps, at the Last Glacial Maximum', *The Cryosphere*, 12(8), pp. 2515–2544. doi: 10.5194/tc-12-2515-2018.
- Creyts, T. T., Clarke, G. K. C. and Church, M. (2013) 'Evolution of subglacial overdeepenings in response to sediment redistribution and glaciohydraulic supercooling', *Journal of Geophysical Research: Earth Surface*, 118(2), pp. 423–446. doi: 10.1002/jgrf.20033.
- Das, B. C. (2022) 'Influence of lithology-controlled hydraulics on pothole evolution', *Acta Geophysica*. Springer International Publishing, (1951). doi: 10.1007/s11600-022-00880-x.
- Dilles, S. ~J. *et al.* (2019) 'Using Global Fiducials High Resolution Imagery, Landsat Imagery, and Sentinel Imagery to Monitor Cyclic Subglacial Draining of Berg Lake, Alaska: 2014 - 2019', in *AGU Fall Meeting Abstracts*, pp. C13C-1317.
- Faber, K. *et al.* (2003) *Geologie und Geotopie im Kanton Schwyz, Berichte der Schweizerischen Naturforschenden Gesellschaft*.
- Fagherazzi, S. *et al.* (2021) 'Bedrock erosion in subglacial channels', *PLoS ONE*, 16(9 September), pp. 1–24. doi: 10.1371/journal.pone.0253768.
- Gilbert, R. (2022) 'Géographie physique et Quaternaire The Devil Lake pothole (Ontario): Evidence of subglacial fluvial THE DEVIL LAKE POTHOLE (ONTARIO): EVIDENCE OF'.
- Hancock, G. S., Anderson, R. S. and Whipple, K. X. (1998) 'Beyond power: Bedrock river incision process and form', in *Geophysical Monograph Series*, pp. 35–60. doi: 10.1029/GM107p0035.
- Hantke, R. (2022) '1152 Ibergereg', in *Geologischer Atlas der Schweiz 1/25 000. Erläuterungen*.
- Hantke, R., Pfiffner, O. A. and Gouffon, Y. (2013) 'Blatt 1172 Muotathal, mit Ostteil von Blatt 1171 Beckenried. – Geol. Atlas Schweiz 1: 25 000, Erläut. 127'.
- Higgins, C. G. (1957) 'Origin of Potholes in Glaciated Regions', *Journal of Glaciology*, 3(21), pp. 11–12. doi: 10.3189/s0022143000024631.
- Holmlund, P. (1988) 'Internal geometry and evolution of moulins, Storglaciaren, Sweden', *Journal of Glaciology*, 34(117), pp. 242–248. doi: 10.1017/S0022143000032305.
- Hooke, R. (1991) 'Positive feedbacks associated with erosion of glacial cirques and overdeepenings', *Geological Society of America Bulletin*, 103(8), pp. 1104–1108. doi: 10.1130/0016-7606(1991)103<1104:PFAWEO>2.3.CO;2.
- Ji, S., Li, L. and Zeng, W. (2018) 'The relationship between diameter and depth of potholes eroded by running water', *Journal of Rock Mechanics and Geotechnical Engineering*, 10(5), pp. 818–831. doi: 10.1016/j.jrmge.2018.05.002.
- Jouvet, G. *et al.* (2021) 'Deep learning speeds up ice flow modelling by several orders of magnitude', *Journal of Glaciology*, 68(270), pp. 651–664. doi: 10.1017/jog.2021.120.
- Jouvet, G. (2023) 'Inversion of a Stokes glacier flow model emulated by deep learning', *Journal of Glaciology*, 69(273), pp. 13–26. doi: 10.1017/jog.2022.41.
- Kale, V. S. and Joshi, V. U. (2004) 'Evidence of formation of potholes in bedrock on human timescale: Indrayani river, Pune district, Maharashtra', *Current Science*, 86(5), pp. 723–726.

- Kamleitner, S. *et al.* (2023) 'Last Glacial Maximum glacier fluctuations on the northern Alpine foreland: Geomorphological and chronological reconstructions from the Rhine and Reuss glacier systems', *Geomorphology*. Elsevier B.V., 423(November 2022), p. 108548. doi: 10.1016/j.geomorph.2022.108548.
- Keller, B. (2021) 'Lake Lucerne and Its Spectacular Landscape', in Reynard, E. (ed.) *Choice Reviews Online*. Cham: Springer International Publishing (World Geomorphological Landscapes), pp. 305–323. doi: 10.1007/978-3-030-43203-4_21.
- Kingslake, J. and Ng, F. (2013) 'Quantifying the predictability of the timing of jökulhlaups from Merzbacher Lake, Kyrgyzstan', *Journal of Glaciology*, 59(217), pp. 805–818. doi: 10.3189/2013JoG12J156.
- Lorenc, M. W., Barco, P. M. and Saavedra, J. (1994) 'The evolution of potholes in granite bedrock, W Spain', *Catena*, 22(4), pp. 265–274. doi: 10.1016/0341-8162(94)90037-X.
- Maisch, M. (2009) 'Geomorphologie und Glaziologie', *Pro Natura Graubünden*, Maloja : B(3), pp. 20–33. doi: <https://doi.org/10.5167/uzh-29054>.
- Meteo Schweiz (no date) *Klima der Schweiz*. Available at: <https://www.meteoschweiz.admin.ch/klima/klima-der-schweiz.html>.
- Nye, J. F. (1959) 'A Method of Determining the Strain-Rate Tensor at the Surface of a Glacier', *Journal of Glaciology*, 3(25), pp. 409–419. doi: 10.3189/s0022143000017093.
- Pelletier, J. D. *et al.* (2015) 'Controls on the geometry of potholes in bedrock channels', *Geophysical Research Letters*, 42(3), pp. 797–803. doi: 10.1002/2014GL062900.
- Reber, R. *et al.* (2014) 'Timing of retreat of the Reuss Glacier (Switzerland) at the end of the Last Glacial Maximum', *Swiss Journal of Geosciences*, 107(2–3), pp. 293–307. doi: 10.1007/s00015-014-0169-5.
- Seguinot, J. *et al.* (2018) 'Modelling last glacial cycle ice dynamics in the Alps', *Cryosphere*, 12(10), pp. 3265–3285. doi: 10.5194/tc-12-3265-2018.
- Shreve, R. L. (1972) 'Movement of Water in Glaciers', *Journal of Glaciology*, 11(62), pp. 205–214. doi: 10.3189/s002214300002219x.
- Werder, M. A. *et al.* (2013) 'Modeling channelized and distributed subglacial drainage in two dimensions', *Journal of Geophysical Research: Earth Surface*, 118(4), pp. 2140–2158. doi: 10.1002/jgrf.20146.
- Werder, M. A. (2016) 'The hydrology of subglacial overdeepenings: A new supercooling threshold formula', *Geophysical Research Letters*, 43(5), pp. 2045–2052. doi: 10.1002/2015GL067542.
- Wohl, E. E. (1998) 'Bedrock Channel Morphology in Relation to Erosional Processes channel morphologies may be divided into multiple or single flowpath', *Geophysica Monograph*, 107, pp. 133–151.

Personal declaration: I hereby declare that the submitted thesis is the result of my own, independent work. All external sources are explicitly acknowledged in the thesis.

Winterthur, 30.09.2023

A handwritten signature in blue ink, appearing to read 'W. Leht.', is positioned above a solid horizontal line. The signature is written in a cursive style.